ARMY RESEARCH LABORATORY

U.S. Army Research Laboratory Directed Energy Visiting Scholars Program 2012 Final Report

by Jeffrey O. White

ARL-TN-0525 **March 2013**

NOTICES

Disclaimers

The findings in this report are not to be construed as an official Department of the Army position unless so designated by other authorized documents.

Citation of manufacturer's or trade names does not constitute an official endorsement or approval of the use thereof.

Destroy this report when it is no longer needed. Do not return it to the originator.

Army Research Laboratory
Adelphi, MD 20783-1197

ARL-TN-0525 **March 2013**

U.S. Army Research Laboratory Directed Energy Visiting Scholars Program 2012 Final Report

Jeffrey O. White
Sensors and Electron Devices Directorate, ARL

REPORT DOCUMENTATION PAGE	Form Approved OMB No. 0704-0188

1. REPORT DATE *(DD-MM-YYYY)*	2. REPORT TYPE	3. DATES COVERED (From - To)
March 2013	Final	February to December 2012

4. TITLE AND SUBTITLE
U.S. Army Research Laboratory Directed Energy Visiting Scholars Program 2012 Final Report

5a. CONTRACT NUMBER

5b. GRANT NUMBER

5c. PROGRAM ELEMENT NUMBER

6. AUTHOR(S)
Jeffrey O. White

5d. PROJECT NUMBER

5e. TASK NUMBER

5f. WORK UNIT NUMBER

7. PERFORMING ORGANIZATION NAME(S) AND ADDRESS(ES)
U.S. Army Research Laboratory
ATTN: RDRL-SEE-M
2800 Powder Mill Road
Adelphi, MD 20783-1197

8. PERFORMING ORGANIZATION REPORT NUMBER
ARL-TN-0525

9. SPONSORING/MONITORING AGENCY NAME(S) AND ADDRESS(ES)
High Energy Lasers Joint Technology Office
Albuquerque, NM

10. SPONSOR/MONITOR'S ACRONYM(S)
HEL-JTO

11. SPONSOR/MONITOR'S REPORT NUMBER(S)

12. DISTRIBUTION/AVAILABILITY STATEMENT
Approved for public release; distribution unlimited.

13. SUPPLEMENTARY NOTES

14. ABSTRACT
Five students participated in U.S. Army Research Laboratory's (ARL's) 2012 summer program for directed energy visiting scholars—two were graduate students; three undergraduates. Their majors include physics, electrical and computer engineering, optical engineering, pure mathematics and computer science. All were not capable of contributing to ARL's high energy laser program; however, they all had the opportunity for a valuable research experience in the areas of lasers, optics, and spectroscopy. Our experience continues to confirm the importance of undergraduate and graduate program to proactively train the future Department of Defense workforce.

15. SUBJECT TERMS
Directed energy, laser diodes, Brillouin spectroscopy, coherent combining, Er:YAG, Brillouin scattering

16. SECURITY CLASSIFICATION OF:			17. LIMITATION OF ABSTRACT	18. NUMBER OF PAGES	19a. NAME OF RESPONSIBLE PERSON
a. REPORT	b. ABSTRACT	c. THIS PAGE			Jeffrey O. White
UNCLASSIFIED	UNCLASSIFIED	UNCLASSIFIED	UU	84	19b. TELEPHONE NUMBER (*Include area code*) (301) 394-0069

Standard Form 298 (Rev. 8/98)
Prescribed by ANSI Std. Z39.18

Contents

1. Introduction 1

2. Recruitment of Participants 1

3. Selection of Participants 1

4. Reporting of Student Research 2

5. Conclusions 2

Appendix A. Using LabView for Test and Automation of ARL Eye-Safe Fiber Laser Testbed 3

Appendix B. Simulation of Stimulated Brillouin Scattering in a Yb Fiber Amplifier 17

Appendix C. Brillouin Scattering and Brillouin Spectroscopy Experiment Design 27

Appendix D. Energy Level Peak Area Calculation for Erbium (Er3+) Yttrium Aluminum Garnet 39

Appendix E. Coherent Combination of Fiber MOPAs Seeded by a Chirped Laser 63

List of Symbols, Abbreviations, and Acronyms 77

Distribution List 78

INTENTIONALLY LEFT BLANK.

1. Introduction

The U.S. Army Research Laboratory (ARL) operated its ninth annual Directed Energy Visiting Scholars program in the summer of 2012, funded by the High Energy Lasers Joint Technology Office (HEL-JTO) and coordinated by the Directed Energy Professional Society (DEPS.) This report summarizes the activities including recruitment, selection among applicants, and research areas pursued. The five technical reports written by the participants are included in the appendices.

2. Recruitment of Participants

Applicants to the summer program were recruited using several methods. A web page describing the program and our team's research topics were posted on ARL's internet site and linked from the DEPS site. We also published a free ad in the Physics Today online classifieds, and asked the physics and electronic engineering (EE) departments at two University of Maryland campuses (College Park and Baltimore County) to post advertisements or circulate via email to their students. Twenty-five students applied; half had credentials of sufficient quality and relevance to warrant serious consideration.

3. Selection of Participants

Twelve applicants were asked to furnish unofficial transcripts and two letters of recommendation; nine students furnished all of the required material. Summer scholar positions were offered to five students; all accepted.

Arayut Amnuaysirikul has a bachelor's degree from the University of Maryland, College Park and is working on a master's degree in software engineering from the University of Maryland, University College (online). He was a good fit for Jun Zhang's need for automating the diode laser testbed.

Shuochen Huang attended U.C. Berkeley for one year; however, because of a large number of Advanced Placement credits, he had junior standing in the Applied Math department. He was a good fit for Jeff White's need for help in adding Yb gain to the MATLAB model of stimulated Brillouin scattering (SBS) suppression in fiber amplifiers.

James Jacobs was a junior majoring in physics and optical engineering at the Rose Hulman Institute of Technology. He was a good fit for helping Jeff White with the project on Brillouin spectroscopy of large mode area (LMA) fibers.

Natalie Kacik, who worked with us in 2011 as well, was one semester away from a bachelor's degree for the School of Electrical and Computer Engineering (ECE) at Cornell. She was a good fit for Larry Merkle's project, which involved analyzing absorption and emission spectra of Er:YAG and Er:Sc_2O_3. She is now in the ECE master's program at Cornell.

Zhi Yi Yang worked with us in 2011, after his first year in the physics master's program at Hunter College of the City University of New York system. This year, after finishing all of the course work required for a master's degree, he chose to work on a project at ARL for the thesis part of the degree. He was a good fit for Jeff White's need for help with the project to coherently combine two erbium fiber amplifiers. Incidentally, Mr. Yang was formerly in the Marine reserves and is a veteran of the Iraq war.

4. Reporting of Student Research

All students submitted summaries of their research to the ARL student colloquium program, three of whom participated in the Sensors and Electron Devices Directorate student intern poster session at summer's end. Final reports were written by all five students.

The primary reporting to the wider community has been the papers given at the Directed Energy Education Workshop. Zhi Yang presented his work in the student session and the unclassified poster session. The full text of each student's report is included in the appendices.

5. Conclusions

We were pleased with the quality of three or four of the DE scholars this year. Students returning for a second year can be beneficial to us; however, during their first year, it is unlikely that even a high-quality sophomore or junior will save us any time. We believe in the importance of training the future Department of Defense workforce and believe that the Directed Energy Visiting Scholars program provides students with an excellent, much-needed, close to real-life learning opportunity. We are pleased to report that one of students from 2010, Christopher Cote, is now applying to graduate school and has decided to change his field from nuclear physics/engineering to optics. He credited his experience here with having a large influence on that.

Appendix A. Using LabView for Test and Automation of ARL Eye-Safe Fiber Laser Testbed

This appendix is presented in its original form without editorial change.

U. S. Army Research Laboratory

SUMMER RESEARCH TECHNICAL REPORT

Using LabView for Test and Automation of ARL Eye-safe Fiber Laser Testbed

Arayut Amnuaysirikul

Mentor: Dr. Jun Zhang

Electro-Optics and Photonics

Sensors and Electron Devices Directorate

Adelphi Laboratory Centre, Maryland

Using LabView for Test and Automation of ARL Eye-safe Fiber Laser Testbed

Amnuaysirikul, Arayut

The Eye Safer Laser Testbed is a state-of-the-art 1.2-kilowatts 1530nm diode pumped fiber laser facility under construction at ARL. It consists of forty fiber coupled diode laser modules, high power multimode fiber combiners, twenty power supplies, and water chillers. LabView program and control electronics are designed and developed and built for the testbed auto operation and monitoring. This presentation includes the design considerations, software and hardware development. Initial results will be presented. Laser interlock safety for the kilowatt power operation is also implemented in the emergency shutdown automation process.

Acknowledgments

The author wishes to acknowledge the mentorship of Jun Zhang, as well as the guidance of John Schill. In addition, the author wishes to express his gratitude for the support given by fellow interns Zhi Yi Yang, Natalie Kacik. Thanks to Jeffrey O. White and Mark Dubinsky for given the opportunity to work at ARL in the summer.

Student Bio

Arayut Amnuaysirikul received the B.S. in Physics from University of Maryland at College Park in 2010 and is currently working toward M.S. degree in Software Engineering at University of Maryland. He plans to graduate with his master degree in 2014, and to join the workforce in software development and communication applications.

1. Introduction/Background

The Eye Safer Laser Testbed at ARL is the state-of the-art multi kilowatts, 1530 nm diode pumped fiber laser facility. It is funded by High Energy Laser (HEL) Joint Technology Office (JTO) and ARL cost-sharing investment. The testbed is to be completed by FY13. This facility is to provide multi kilowatts diode-pump source for the power scaling of ARL low quantum-defect, resonantly pumped Erbium fiber laser research work. Additionally, it serves as a general platform of the eye safer wavelength to the HEL communities. This report lays out the design architecture and considerations of the construction of the testbed. Over 310 W of combined 1530 nm power out of 105/125 μm multimode fiber has been demonstrated. The laser characteristics and performance of the testbed is also described.

2. Design

The testbed is mainly divided into three component parts: LabView control, power sources, and water chiller. The first component is the LabView control. The major function is to control twenty power supplies and monitor current and voltage of each diode. In addition, it operates for monitoring and shutting down the power supplies when somebody tries to break the interlock and the event of an emergency such as a power failure. The second component is the power sources; they directly send current and voltage to power up the laser diodes. Each power supply has power to operate up to two laser diodes. The third component is the water chiller, which dissipates the buildup heat and maintains the temperature of the entire system. These three major components connect to fiber laser diodes that are combined to the pump coupler. Then, it outputs 1–2 kW pump to FBG optics.

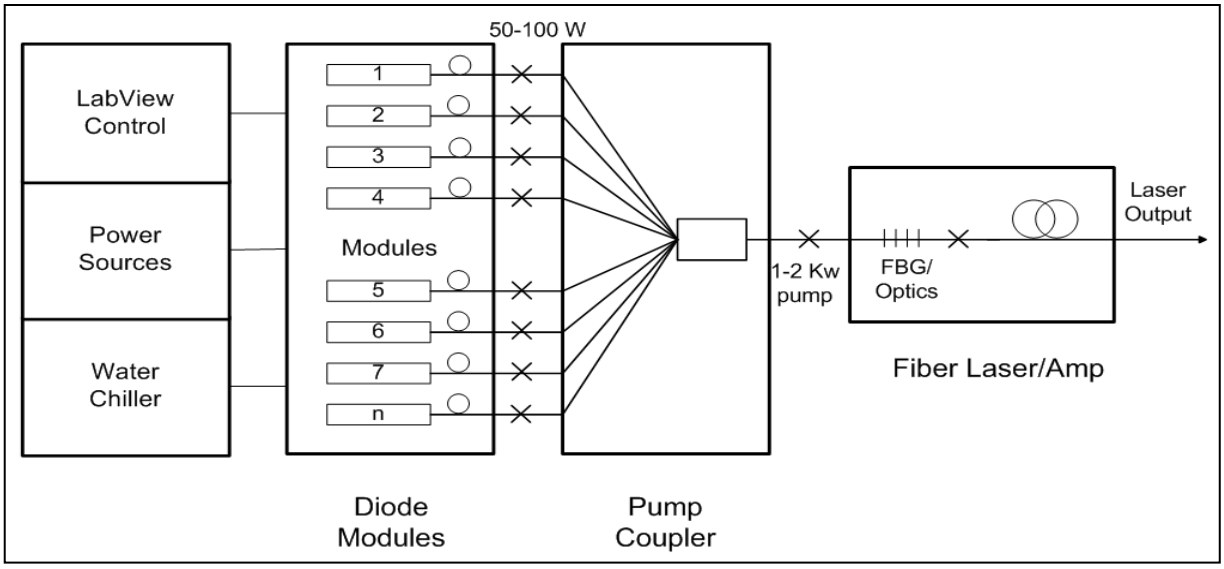

Figure 1. Design schema of eye safe fiber testbed.

3. Hardware Control

3.1 Power sources

There are a total of twenty power supplies connected in the daisy-chain connection. Each power supply is capable of powering up to 1.5 kW, and the maximum output current is 12 A. In order for these power supplies to communicate throughout the testbed, we must create a unique address to each power supply by naming each unit by some number (from 1-31). Only the first unit is connected to the PC via RS 232, and other units were connected via a RS 485 interface. These are linked using RS 232/485 cable from "in" position to "out" position.

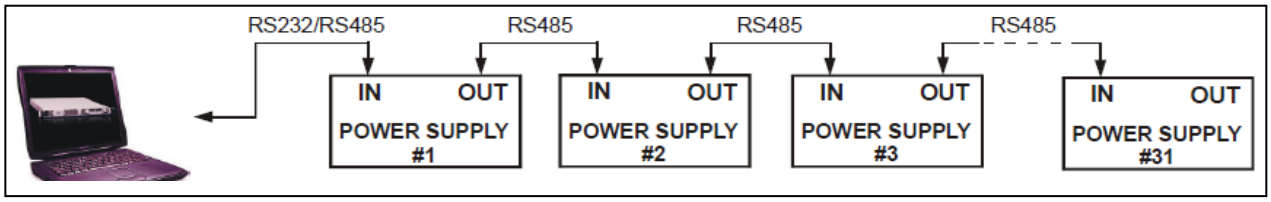

Figure 2. Power supplies connected in the daisy-chain connection.

Figure 3. Front panel of power supplies.

Figure 4. Back panel RS485 linked “IN” to “OUT” position .

3.2 Water Chiller

The water chiller module also plays a major function in the testbed because without sufficient cooling power the whole procedure in the test will collapse. The LYTRON water chiller is proficient to cool down forty diode lasers simultaneously. The specification of the water chiller is: capacity of 5,900 watts at 20° c delivery water and 20° c ambient temperature; the cooling temperature range is +5°c to +35°c.

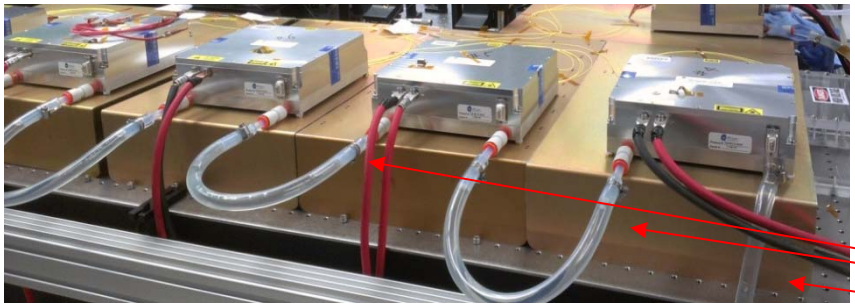

Water chiller hoses connect one end of the unit and chain to another one.

Figure 5: Water chiller.

4. Software Control

4.1 LabView Automation

The operation on LabView is a crucial part of the experiment because it monitors and examines the status of the individual power supply. First, select the VISA Input to COM1. Then select the GEN Address and Baud rate. After that enter the voltage and current number into the configuration box and select RUN the LabView. On the front panel there is a summary table for

voltage and current that updates information regarding each power supply. Moreover, the table contains the error status that warns of any abnormal behavior if a failure takes place.

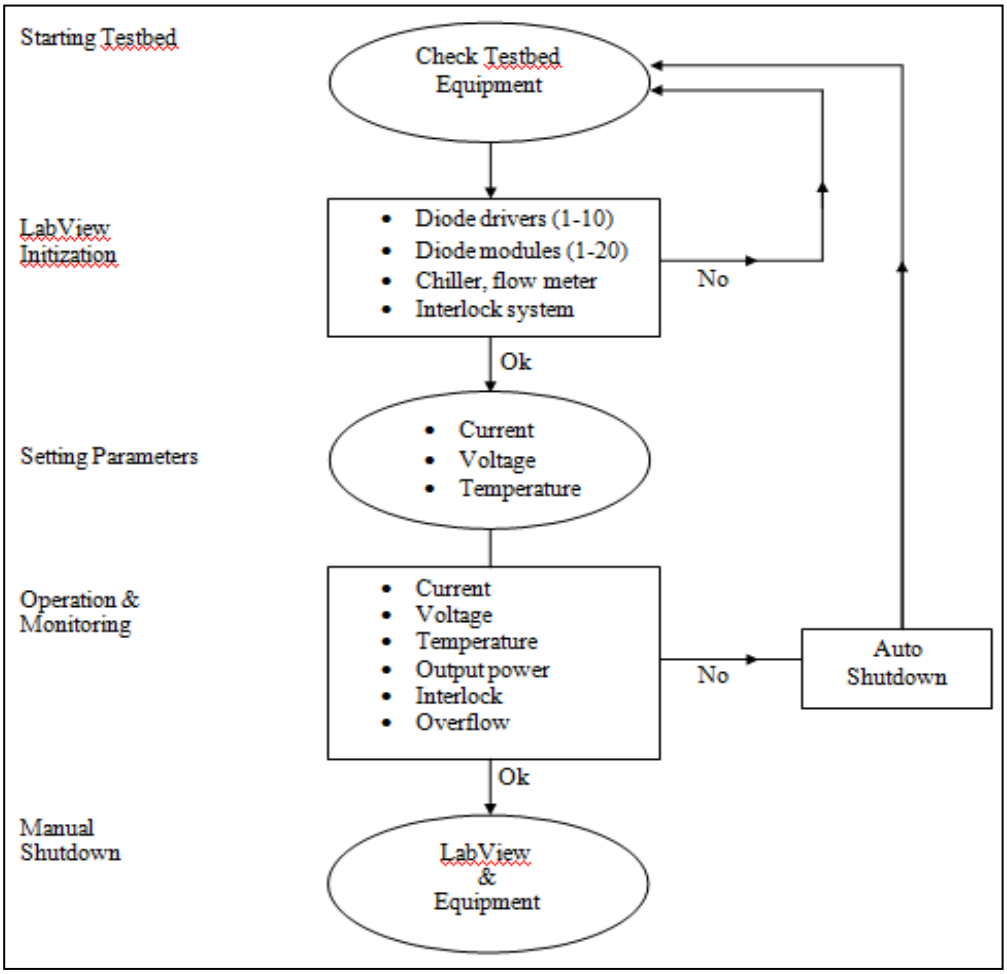

Figure 6. Testbed flow diagram.

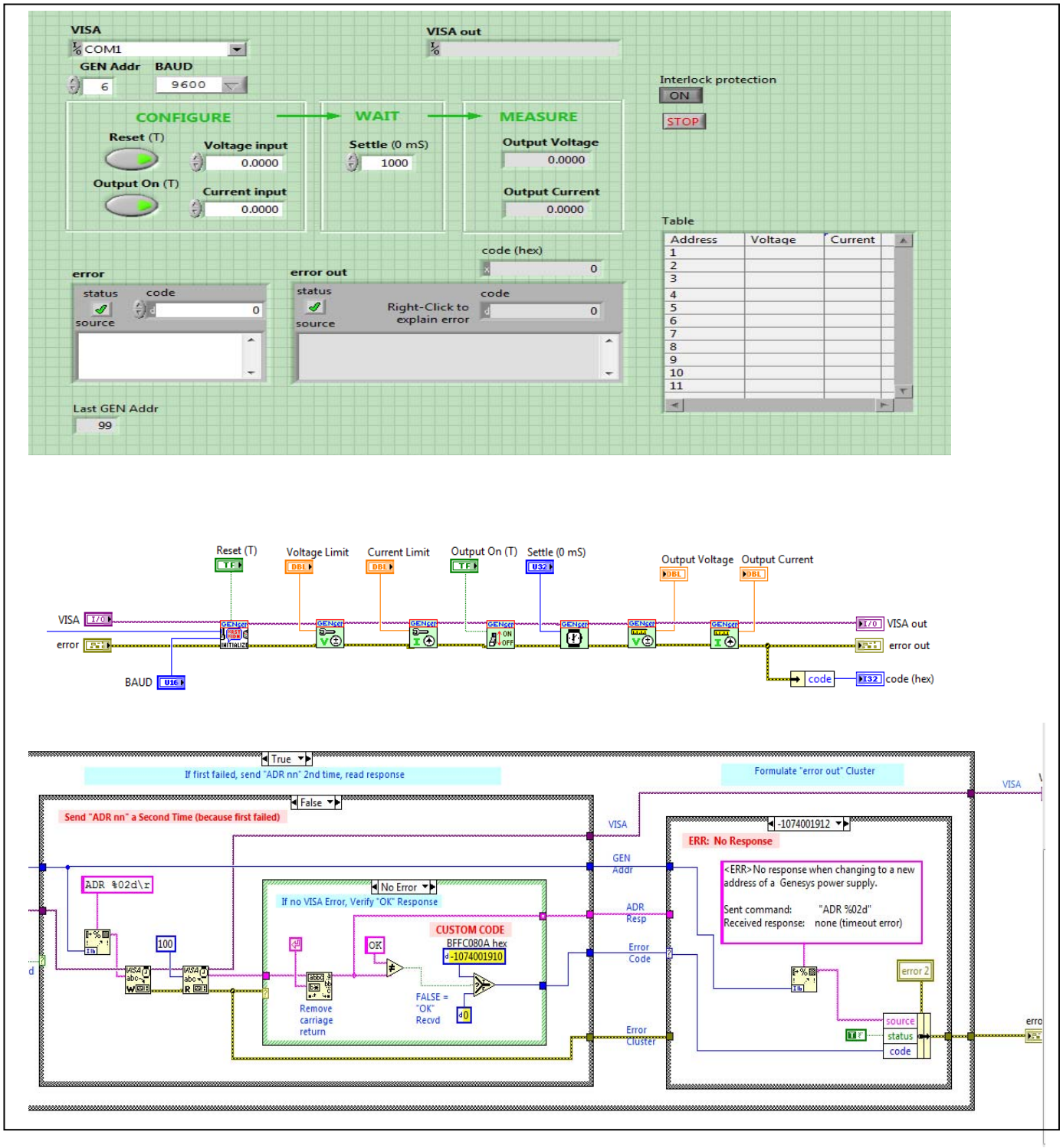

Figure 7. Block diagram.

4.2 Interlock System

The interlock protection is constructed as part of LabView control. If someone accidently breaks into the lab, the interlock protection activates and disables the power supplies by reseting the current and voltage to zero. Also, there is the stop button for manuel resetting of the interlock.

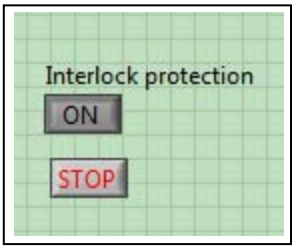

Figure 8. Interlock.

4.3 General Procedure

The process begins:

1. Check all equipment such as power supplies, laser diodes, water chiller, hoses, and cable.
2. Turn on LabView and begin to input the parameters; if there is an error, it will shut down all the power supplies.
3. Continue the operation of and monitoring by the LabView software; it will begin to shut down the testbed in the event of a false situation, for example, an unusual level of current or voltage, interlock breaking, or abnormal output power.
4. If everything works perfectly, let the test manually shutdown the LabView and equipment.

5. Summary and Conclusions

In this project, I had learned and understood how to operate the Eye Safer Fiber Testbed. During the first couple week I had to find all the necessities parts such as the power cables and make a cable that connects from the PC to the power supplies. Furthermore, the project did not have any actual data because it is still in the development stage and waiting for the funding. However, in the near future I will try to add more software detail to indicate temperature and overflow rate for each laser diode.

6. References

1. Bishop, H. Robert. *LabView 7 Express Student Edition.* Upper Saddle, N.J.: Pearson Prentice Hall, 2006, P.114–150.
2. "Lytron." About. N.p., n.d. Web 20 July 2012. <http://www.lytron.com/About-Lytron>.
3. Serway, Raymond A.; Moses, Clement J.; Moyer. Curt A. *Modern Physics.* Philadelphia: Saunders College, 1989.
4. *Technical Manual for GENESYS™ 750W-1500W*. TDK-Lambda America, Inc.

INTENTIONALLY LEFT BLANK.

Appendix B. Simulation of Stimulated Brillouin Scattering in a Yb Fiber Amplifier

This appendix is presented in its original form without editorial change.

U. S. Army Research Laboratory

SUMMER RESEARCH TECHNICAL REPORT

Simulation of Stimulated Brillouin Scattering in a Yb Fiber Amplifier

Shuochen Huang

Mentor: Dr. Jeffrey O. White

Electro-Optics and Photonics

Sensors and Electron Devices Directorate

Adelphi Laboratory Center, Maryland

Simulation of Stimulated Brillouin Scattering in Yb Amplifier Fiber

The simulation of stimulated Brillouin scattering, built in Matlab, models three partial differential equations describing the behavior of the laser wave, the Stokes wave, and the acoustic wave with respect to time and space; and two ordinary differential equations describing the behavior of the diode pump with respect to space and fractional inversion of ytterbium with respect to time. It was determined that using Heun's method, an improvement over Euler's method, causes an error that scales inverse quadratically with the number of iterations while requiring less than 50% additional computation time. In addition, the evaluation of the three partial differential equations along their lines of characteristics rather than along the time axis, as was explored previously in another simulation, cuts down computation time by approximately 50%. The effects of different chirps and different amounts of input diode pump power on SBS and laser power output are examined.

Acknowledgments

This project could not have reached its current state without the mentorship and guidance of Dr. Jeffrey White. The author would also like to thank Dr. Carl Mungan and Dr. Eliot Petersen for providing much needed assistance and instruction throughout the summer.

Student Bio

Shuochen Huang graduated from high school in 2010 and is pursuing a Bachelors of Arts at the University of California, Berkeley, double majoring in pure mathematics and computer science. He plans to graduate in the spring of 2014 and pursue graduate studies.

1. Introduction/Background

A mathematical model must balance the trade off between runtime and accuracy. A numerical method that runs appropriately rapidly and produces appropriately accurate results must be chosen. The program itself must be molded to fit the strengths of Matlab to maximize efficiency. Most importantly, the results of the simulation should match empirical results obtained from experiments. Stimulated Brillouin scattering (SBS) is a phenomenon that limits the output power of fiber lasers. Although fiber lasers are more compact and reliable than other types of lasers, the problem of stimulated Brillouin scattering must be conquered before high power fiber lasers can be used by the Army for directed energy applications. The simulation models the effects of ytterbium doping and signal chirping in mitigating the effects of stimulated Brillouin scattering.

2. Modeling

The simulation approximates solutions to the following equations, describing SBS in a fiber laser with Yb amplifier (*1*, *3*).

$$\frac{\delta E_L}{\delta z} + \frac{n}{c}\frac{\delta E_L}{\delta t} = -\frac{\alpha_L}{2}E_L + i\kappa E_S\rho$$

$$\frac{\delta E_S}{\delta z} - \frac{n}{c}\frac{\delta E_S}{\delta t} = \frac{\alpha_L}{2}E_L - i\kappa E_S\rho'$$

$$\frac{\delta P_D}{\delta z} + \frac{n}{c}\frac{\delta P_D}{\delta t} = \alpha P_D$$

$$\frac{\delta \rho}{\delta t} + \frac{\Gamma}{2}\rho = i\Lambda E_L E_S' + f$$

$$\frac{\delta n}{\delta t} = \frac{\sigma_{pe}N_{Yb}P_D n}{h\nu_p A_p} - \frac{\sigma_{se}N_{Yb}P_L n}{h\nu_s A_L} - \frac{n}{\tau_{Yb}} + \frac{(1-n)P_D N_{Yb}\sigma_{pa}}{h\nu_p A_p} + \frac{(1-n)P_L N_{Yb}\sigma_{sa}}{h\nu_s A_L}$$

E_L and E_S represent the laser and Stokes fields. P_D and P_L represent the diode and laser powers. κ and Λ are the Brillouin coupling coefficients, Γ is the phonon decay rate, and f represents the thermal density that cause the initial Brillouin scattering. Q is the noise constant that determines the strength of the noise. n is the fractional inversion. N_{Yb} is the ytterbium number density. τ_{Yb} is the excited state lifetime of ytterbium. α subscript D and L are gain or loss coefficients for diode and laser. A subscript L and D are effective areas of laser and diode modes. The method of characteristics reduces the partial differential equations to ordinary differential equations, decreasing computation time (*2*).

3. Results and Discussion

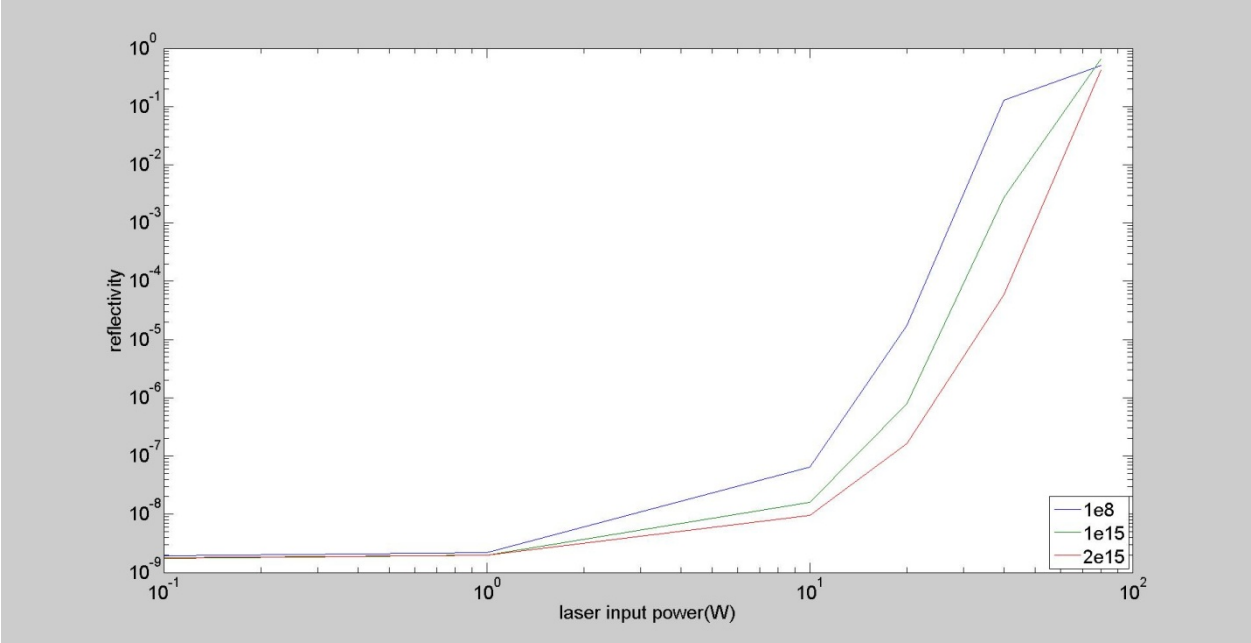

Figure 1. This is a graph of power reflected by SBS against laser input power. It is clear that chirp suppresses SBS and higher chirp causes less laser power to be reflected back.

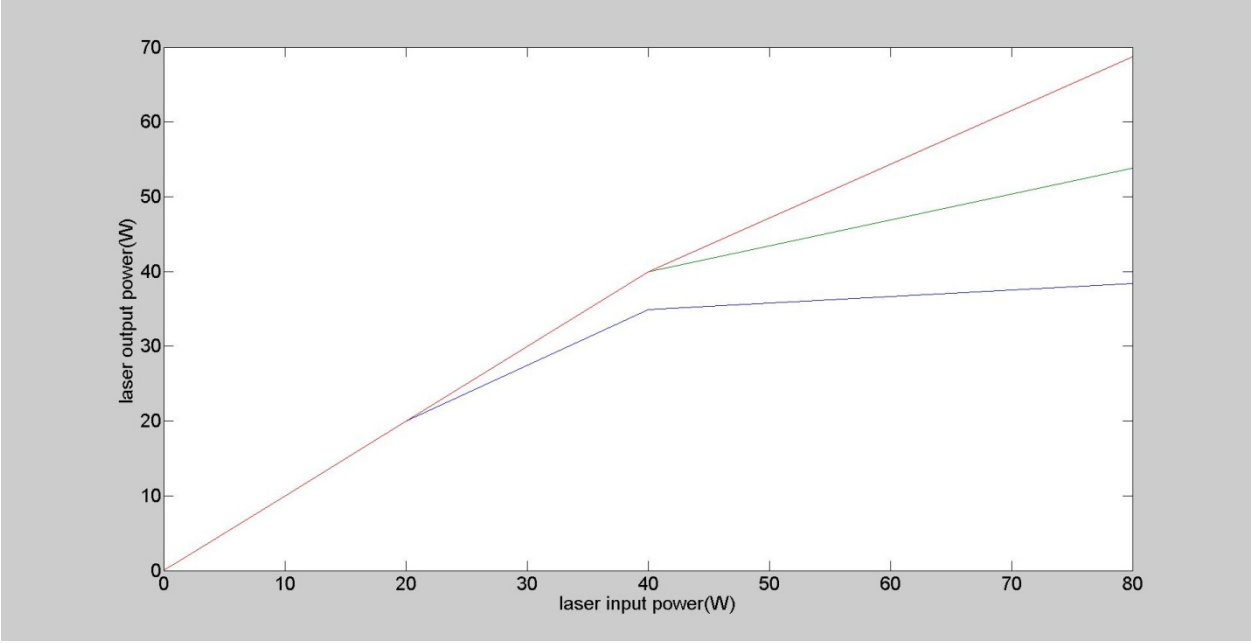

Figure 2. This is a graph of the same data, showing laser output power against laser input power. Higher chirp causes more laser power to be outputted.

4. Summary and Conclusions

This simulation offers insight into the effects of ytterbium amplifiers and chirping on producing high power fiber lasers and mitigating stimulated Brillouin scattering. Its results can be compared against the results of experiments. Unfortunately, the simulation does not accurately model laser gain in active fibers. Further improvements can be made in optimizing the program. For example, the technique of cache blocking, which keeps the data in the computer that is being worked on the most at the highest strata of memory, thus reducing time spent on retrieving information from memory, can be used to improve runtime. The simulation can be made to model experiments more closely by taking into account the varying amounts of ytterbium in the fiber rather than assuming a constant density.

5. References

1. David, A.; Horowitz, M. Low-frequency Transmitted Intensity Noise Induced y Stimulated Brillouin Scattering in Optical Fibers. *Optics Express* **June 2011**, *19* (12).
2. Damzen, M.; Hutchinson, H. Laser Pulse Compression by Stimulated Brillouin Scattering in Tapered Waveguides. *IEEE Journal of Quantum Electronics* **January 1893**, *QE-19* (1).
3. Wright, M.; Valley G. Yb-Doped Fiber Amplifier for Deep-Space Optical Communications. *Journal of Lightwave Technology* **March 2005**, *23* (3).

INTENTIONALLY LEFT BLANK.

Appendix C. Brillouin Scattering and Brillouin Spectroscopy Experiment Design

This appendix is presented in its original form without editorial change.

U. S. Army Research Laboratory

SUMMER RESEARCH TECHNICAL REPORT

Brillouin Scattering and Brillouin Spectroscopy Experiment Design

James Jacobs

Mentors: Eliot Petersen, Jeffrey O. White

Electro-Optics and Photonics

Sensors and Electron Devices Directorate

Adelphi Laboratory Center, Maryland

Abstract

Fiber lasers have been proposed as a method to protect soldiers from rockets, artillery shells, mortars and other forms of enemy armaments, as their small form factor, light weight, and high wall plug efficiency make them very attractive. One consistent problem lies in stimulated Brillouin scattering (SBS) in fiber amplifiers and delivery fiber, which causes lower power output due to backwards scattering on acoustic modes within the fiber. The onset of SBS scales with input power and fiber length and for laser power beyond threshold a large fraction of the forward propagating power can be scattered backwards. By measuring the backward scattered homogeneous and inhomogeneous SBS bandwidth we can more accurately model and characterize Brillouin scattering in fibers for future experiments and models. Experiments were designed to observe and characterize these important effects.

Acknowledgments

The author wishes to acknowledge the mentorship of Drs. Eliot Petersen and Jeffrey O. White. Thanks to Dr. Jeffrey O. White for the opportunity to work at ARL this summer.

Student Bio

James Jacobs is currently a senior at Rose-Hulman Institute of Technology working toward a Bachelors of Science degree in Physics and Optical Engineering. He plans to attend graduate school following completion of his undergraduate studies.

1. Introduction/Background

Brillouin scattering and stimulated Brillouin scattering is a source of many issues in high power fiber laser applications. In order to understand it better, we can characterize the SBS bandwidth. Two primary types of SBS broadening exist: inhomogeneous and homogeneous broadening. Inhomogeneous SBS broadening occurs in long lengths of fiber due to slight variations of core size, doping concentrations, and other parameters over the length of the fiber, while homogeneous SBS broadening is the fundamental bandwidth associated with the acoustic phonon lifetime.[1] Knowing more information about the effects of Brillouin scattering will help more accurately model and characterize SBS for future experiments and models.

2. Theory

The main goal of the experiment is to determine the bandwidth of the SBS gain. In order to create the SBS effects in the fiber, two lasers are used: one as a "pump" laser and the other as a tunable "probe" laser. The "pump" laser does exactly that – it pumps the fiber at a high energy output to create the electrostriction necessary in the fiber, which in turn generates acoustic vibrations that scatter the beam in the opposite direction. The scattered beam experiences a frequency shift due to the energy lost from the phonons creating the acoustic waves.[2] The second laser, the "probe" laser, is scanned around the frequency that the pump laser light shifts to. When the probe and shifted pump light are within the appropriate range to interfere, they will constructively interfere to produce gain within the fiber. This gain can be detected by an increase in intensity of the output signal of the probe laser, and the SBS gain bandwidth can be determined by scanning the probe over the frequencies within the SBS gain bandwidth.

3. Brillouin Scattering Experiment

Using a single laser, Brillouin scattering can be observed. By sending the laser down a long length of single mode fiber, the backscattered light can be observed to emerge from where it entered.

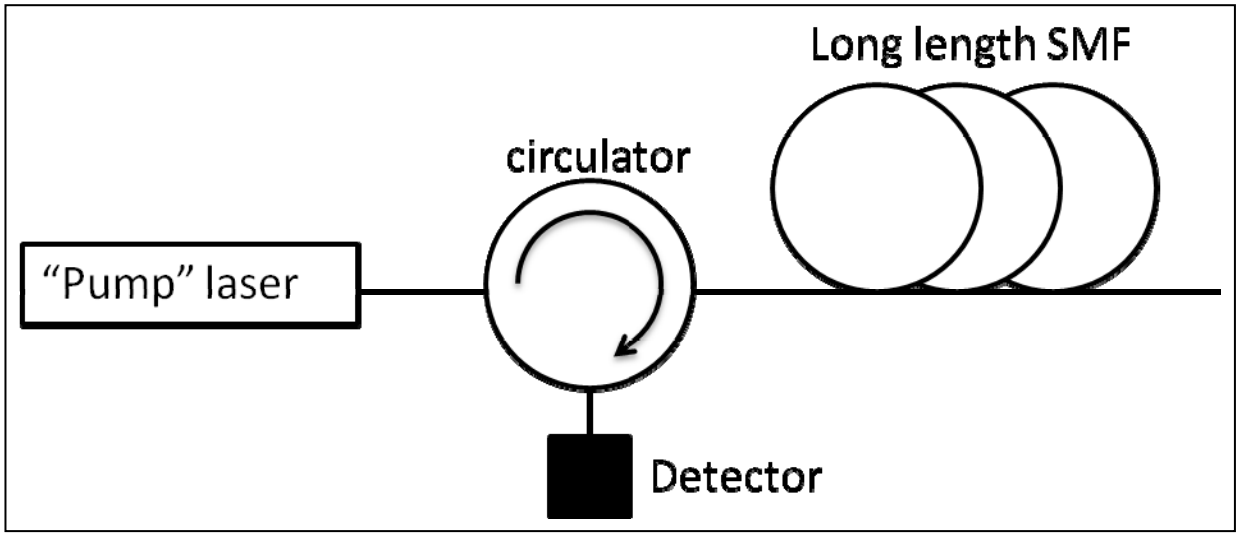

Figure 1. Brillouin scattering experimental setup.

A circulator was utilized to avoid light getting back to the laser and damaging it and to direct the backscattered light into the detector. Data was first taken for the power output of the laser by itself, which is the power going into the long length of single mode fiber that helps create the backscattered light. Data was then taken utilizing the circulator and long length of single mode fiber to see the power level of the backscattered light created by the laser.

4. Brillouin Scattering Data and Analysis

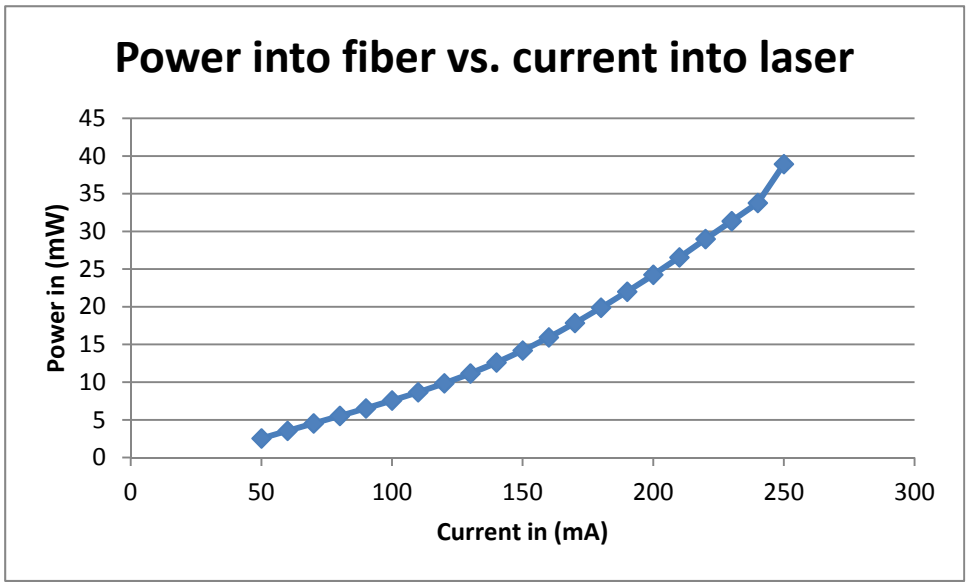

Figure 2. Power into fiber vs. current into laser.

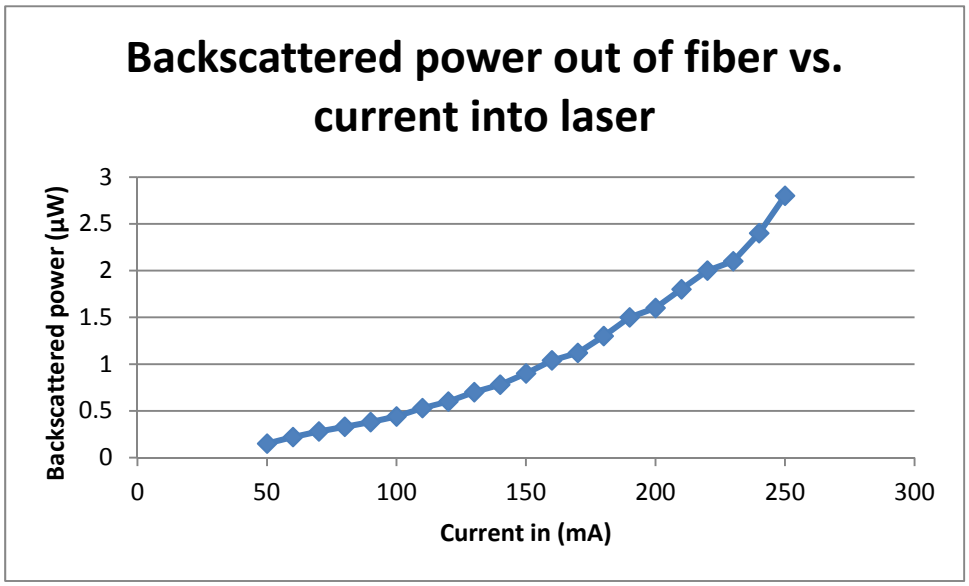

Figure 3. Backscattered power out of fiber vs. current into laser.

From figures 2 and 3 alone, we can already see that the backscattered power follows nearly the exact same pattern as the power input into the laser when plotted as a function of current.

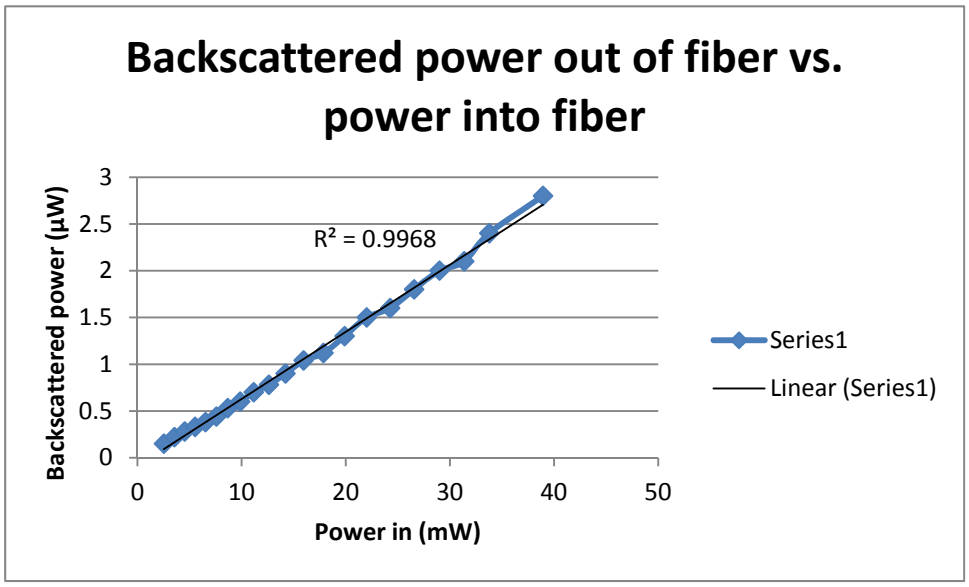

Figure 4. Backscattered power out of fiber vs. power into fiber.

Figure 4 shows how the backscattered power scales very close to the power input into the fiber, with an R^2 value of 0.9968 – very nearly a linear fit.

This linearity seen in figure 4 is an indication that spontaneous Brillouin scattering is occurring in the fiber rather than stimulated Brillouin scattering. In the case of stimulated Brillouin

scattering, the backscattered light is much higher and is non-linearly related to the input power (*3*).[3]

5. SBS Bandwidth Determination Experiment Design

In order to determine the SBS bandwidths, an experiment was designed utilizing a pump – probe system.

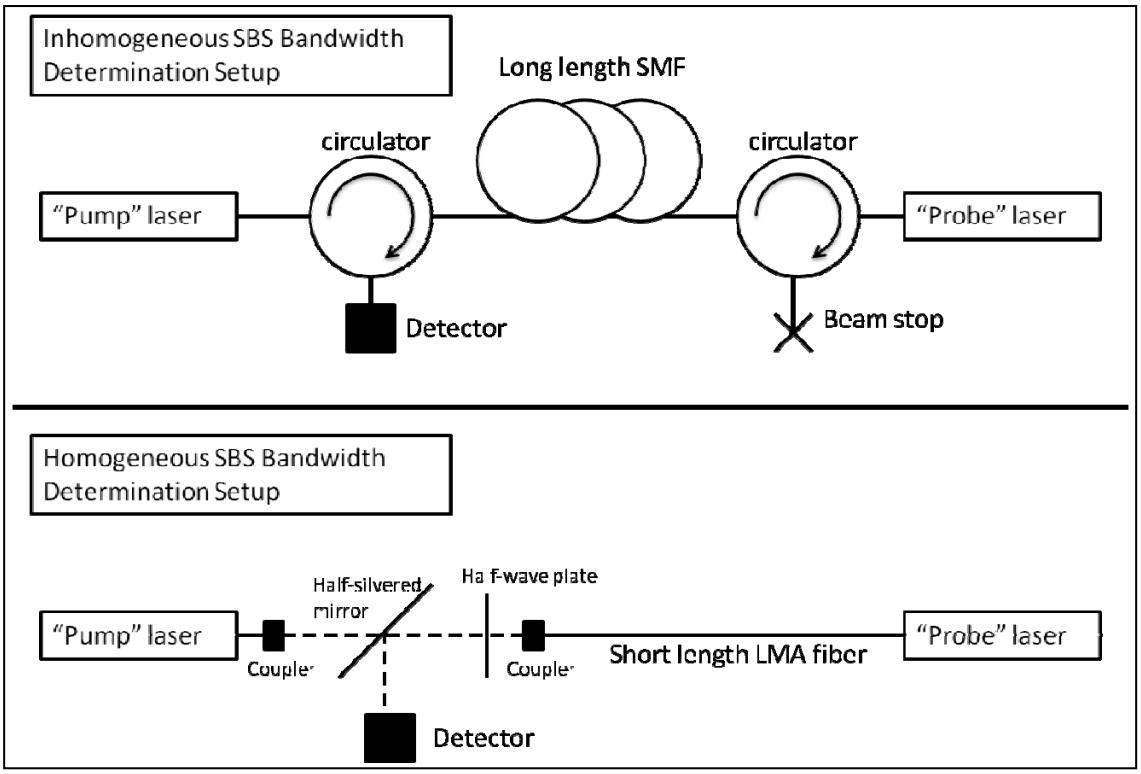

Figure 5. SBS Bandwidth determination experimental setups.

Both experiments are designed to prevent any damage to the laser itself due to incoming light, with the inhomogeneous setup utilizing circulators and the homogeneous setup using a half-wave plate and polarizer to stop back reflections. The homogeneous bandwidth determination setup also utilizes free space optics (indicated by the dotted lines) due to the necessity to couple light into LMA fibers due to core size differences.

As for the detector, a scanning Fabry-Perot Interferometer (FPI) connected to an oscilloscope to view the spectrum yields the highest resolution in terms of frequency, which is necessary for the narrow band at which SBS gain is evident (~50 MHz).

After setting up the experiment, the pump laser should be set to an appropriate power to generate SBS in the fiber. The probe laser should then be scanned at any power level that is safe for the

detector at the frequencies at which the gain should be evident (~11 GHz from the pump frequency over a range of ~50 MHz).[3]

6. Conclusions and Recommendations

Brillouin scattering can be observed in fiber with high enough laser power. The backscattered power scales very closely to the power input into the fiber, with an R^2 value of 0.9968 for a linear fit. This linearity proves that it is spontaneous rather than stimulated Brillouin scattering, which would demonstrate non-linear effects.

The experiment design presented is useful for gathering data on both inhomogeneous and homogeneous SBS broadening for comparison and determination of the bandwidths at which gain occurs.

7. References

1. Bass, Michael.; Mahajan, Virendra N.; Van Stryland, Eric. Handbook of Optics: Design, Fabrication, and Testing; Sources and Detectors; Radiometry and Photometry. McGraw Hill Professional. p. 16.5, 2009.

2. Tkach, R. W.; Chraplyvy, A. R.; Derosier, R. M. Spontaneous Brillouin Scattering for Sngle-mode Optical-fibre Characterisation. *Electronics Letters* **September 11-1986**, *22* (19), 1011–1013.

3. Yeniay, A.; Delavaux, J.; Toulouse, J. Spontaneous and Stimulated Brillouin Scattering Gain Spectra in Optical Fibers. *J. Lightwave Technol.* **2002**, *20*, 1425.

INTENTIONALLY LEFT BLANK.

Appendix D. Energy Level Peak Area Calculation for Erbium (Er3+) Yttrium Aluminum Garnet

This appendix is presented in its original form without editorial change.

U.S. Army Research Laboratory

SUMMER RESEARCH TECHNICAL REPORT

Energy Level Peak Area Calculation for Erbium (Er^{3+}) Yttrium Aluminum garnet (YAG)

Natalie Kacik
Mentor: Dr. Larry Merkle
Microphotonics Branch, Sensors and Electron Devices Division, Adelphi Laboratory Center

Abstract

The U.S. Army has a program dedicated to the creation of power-scalable solid state lasers. Essential to the design of these lasers, is the ability to predictably select materials that are eye safe and optimal for lasing. The goal of our research is to collect and fit the peak cross sections of erbium (Er^{3+}): yttrium aluminum garnet (YAG) and Er: scandium oxide ($Sc_2O_{3)}$. Ultimately, the fits will be used by a colleague to develop theory that can explain why one type of crystal material is better for lasing than another.

Acknowledgments

The author wishes to acknowledge the mentorship of Dr. Larry Merkle

Student Bio

Natalie Kacik graduated with her B.S. in Electrical and Computer Engineering at Cornell University last spring and will continue in pursuit of her Masters of Engineering in ECE this fall. Last summer Natalie interned at ARL where she worked under Dr. Jeffrey O. White and wrote a model for Stimulated Brillouin Scattering in a Fiber Amplifier.

1. Introduction/Background

Er:YAG and Er:Sc_2O_3 are two promising laser materials that can be used for military applications. An important factor in determining whether a material can be used for lasers is the proximity in wavelength between absorption and stimulated emission peaks as well as their relative gain. Ideally, an emission and absorption peak will be close in wavelength so that less energy will be lost due to the change in wavelength between the peaks and more energy can be converted to emitted light. Furthermore, it may be advantageous to cryogenically cool the lasing material because it causes the laser peaks to narrow and heighten. To use the material as a laser, it will need to be stimulated by a beam at a wavelength where the absorption is less than the emission peak. In this project, the absorption cross section peak areas for Er:YAG and Er: Sc_2O_3 were calculated at 7K to find the relative strength of each peak. The rest of this technical report will refer to the experimental results of Er: YAG. However, similar procedures were done in collecting the data for Er: Sc_2O_3.

2. Experiment/Calculations

Absorbance spectra were taken using an Agilent Technologies Cary 6000i spectrophotometer that uses an InGaAs detector and photomultiplier. The spectra data ranged from 200–1550 nm with a slit width of 0.2 nm for room temperature and 0.1 nm for all temperatures below room temperature. The Er:YAG sample has a thickness of 0.283 cm and a calculated Er concentration of 6.94×10^{19} cm^{-3}. To calculate the absorption cross section from the absorbance data the following conversions were used:

$$\alpha = \frac{-Ln(10^{-A})}{L} \qquad (Eq.\,1.1)$$

Where α is absorption coefficient(cm^{-1}), A is absorbance and L(cm) is the thickness of the sample. Absorption is converted to cross section using the equation:

$$Absorption\ Cross\ Section = \frac{\alpha}{Er_{concen}} \qquad (Eq.\,1.2)$$

After calculating the absorption cross section and correcting for baseline, either a Gaussian or Lorentzian fit was used for each peak. The equation for the Gaussian peak is:

$$G(x) = \frac{e^{-(\nu-\nu_0)^2/2\sigma^2}}{\sigma\sqrt{2\pi}} \qquad (\text{Eq. } 1.3)$$

And the equation for the Lorentzian linewidth is

$$L(x) = \frac{\nu_{FWHM}}{2\pi\left[\left(\frac{\nu_{FWHM}}{2}\right)^2 + (\nu - \nu_0)^2\right]} \qquad (Eq.\ 1.4)$$

Where σ is the standard deviation, ν_0 is the wavelength at a peak and ν_{FWHM} is the Full Width Half Max.

3. Results and Discussion

The 1513–1517 nm range fit, representing a portion of the $^4I_{13/2}$ manifold in Er and the eye-safe region at 8K, is shown in figure 1 below. (The full set of graphs are included in the appendix)

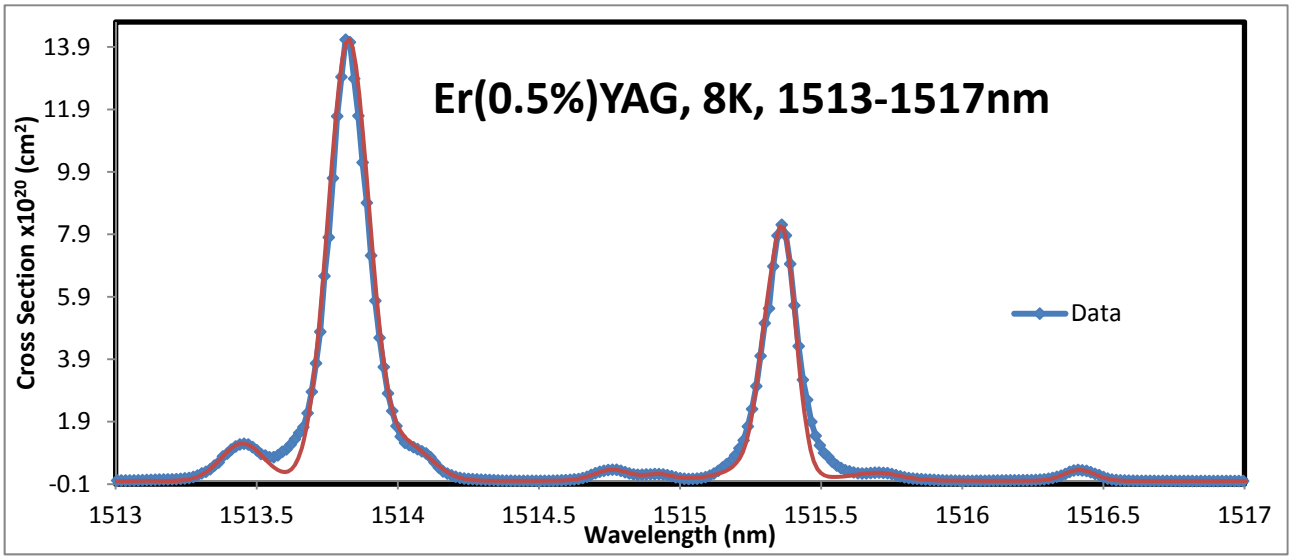

Figure 1. Absorption (blue) spectra and fit (red) of Er: YAG sample at 8K from 1513–1517 nm.

There were some wavelength ranges in the data where neither a Lorentzian nor Gaussian profile could fit. Two such sites are shown in figure 1 at 1513.7 nm and 1515.5 nm. These peaks could not be resolved because of their close proximity to another peak. There were other peaks where a Voigt profile may have been a better fit, and a couple of peaks that were from minority sites on the crystal, and, therefore, could not be reliably differentiated from the noise level. Examples of such peaks can be seen in the appendix. If a peak could be reasonably defined, the best fit Gaussian or Lorentzian profile was used. Irresolvable peaks were not fitted. The integral of the cross section over wavelength was calculated for each fitted peak. This value is directly proportional to the strength of the transition at that wavelength. An excerpt from the original table of peak areas is shown below. (The full table is included in the appendix)

Table 1. Lines believed to come from true ground state of Er^{3+} in YAG.

	Absorption strengths and transition energies – 8K – Er:YAG							
Final manifold	No.	λ (nm)	σ_{expt} (10^{-20} cm^2)	Line width (nm FWHM)	Area under $peak_{expt}$ (10^{-20} cm)			
$^4I_{13/2}$		1526.87	9.3	0.15	9.4			
		1515.36	7.4	0.11	3.8 *			
		1513.83	14	0.17	11			
		1473.58	4.8	0.40	14			
		1469.36	14	0.38	38			
		1452.32	9.4	1.0	70			
		1451.2	very	weak	shoulder			

Table 2. Lines probably due to absorption from higher-lying states of $^4I_{15/2}$ (but may also include minority site peaks and/or vibronics).

	Absorption strengths and transition energies – 8K – Er:YAG							
Final manifold	No.	λ (nm)	σ_{expt} (10^{-20} cm^2)	Line width (nm FWHM)	Area under $peak_{expt}$ (10^{-20} cm)			
$^4I_{13/2}$		1532.13	2.0	0.12	1.1 *			
		1531.00	0.16	0.13	0.10			
		1527.55	0.23	0.14	0.15			
		1526.47	0.21	0.12	0.12			
		1526.32	0.18	0.14	0.11			
		1525.89	0.22	0.15	0.15			
		1525.45	0.19	0.16	0.13			
		1518.99	0.14	0.17	0.16			
		1516.42	0.35	0.13	0.21			
		1515.70	0.23	0.19	0.20			
		1515.29	2.4	0.10	1.7 **			
		1514.76	0.34	0.15	0.24			
		1514.04	1.1	0.20	1.0			

		1513.45	1.2	0.18	1.0			
		1510.32	0.39	0.14	0.26			
		1478.48	0.29	0.35	0.73			
		1474.22	0.64	0.29	1.3			
		1466.80	0.16	0.35	0.40			
		1466.46	0.18	0.39	0.35			
		1457.16	0.19	1.0	0.95			
		1447.00	0.04	0.90	0.18			

* Area under peak may be in error by more than 10% due to finite resolution of instrument

** Area under peak may be in error by more than 30% due to finite resolution of instrument

4. Summary and Conclusions

We measured the absorbance spectra of Er:YAG and Er:Sc_2O_3 and fitted the peak absorption cross sections to either a Gaussian or Lorentzian linewidth. The area under each peak was found and matched to its corresponding manifold.

5. References

Gruber, J.; Nijar, A.; Sarder, D. K.; Yow, R.; Russell III, C.; Allik, T.; Zandi, B. Spectral Analysis of Energy-Level Structure of $Er^{3+}(4f^{11})$ in Polycrystalline Ceramic Garnet $Y_3Al_5O_{12}$. *J Appl Phys* **2005**, *97*, 3–4.

Gruber, J.; Quagliano, J. R.; Reid, M. F.; Richardson, F. S.; Mills, M. E.; Seltzer, M. D.; Stevens, S. B.; Morrison, C. A.. Allik, T. H. Energy Levels and Correlation Crystal-field Effects in Er3+-doped Garnets. *Phys Rev B* **1993**, *48*, 15567–15569.

Merkle, L. D.; Ter-Gabrielyan, N. *Host-Dependence of Trivalent Erbium (Er3+) Spectra Relevant to Solid-state Lasers: Yttrium Aluminum Garnet (YAG) and Sesquioxides*; ARL-TR- 5755 1-7; (2011).

6. Appendix List of Figures/Tables

Figure a.1 Absorption (blue) spectra and fit (red) of Er: YAG at 8K from 200-430nm……..9

Figure a.2 Absorption (blue) spectra and fit (red) from Er: YAG at 8K from 229-261nm.…10

Figure a.3 Absorption (blue) spectra and fit (red) from Er:YAG at 8K from 252-261nm…..10

Figure a.4 Absorption (blue) spectra and fit (red) of Er: YAG at 8K from 271-288nm.……11

Figure a.5 Absorption (blue) spectra and fit (red) of Er: YAG at 8K from 430-750nm.……11

Figure a.6 Absorption (blue) spectra and fit (red) of Er: YAG at 8K from 440-452nm.……12

Figure a.7 Absorption (blue) spectra and fit (red) of Er: YAG at 8K from 482-489nm.……12

Figure a.8 Absorption (blue) spectra and fit (red) of Er: YAG at 8K from 514-545nm.……13

Figure a.9 Absorption (blue) spectra and fit (red) of Er: YAG at 8K from 643-656nm.……13

Figure a.10 Absorption (blue) spectra and fit (red) of Er: YAG at 8K from 780-800nm.…..14

Figure a.11 Absorption (blue) spectra and fit (red) of Er: YAG at 8K from 957-1100nm.…14

Figure a.12 Absorption (blue) spectra and fit (red) of Er: YAG at 8K from 1455-1480nm…15

Figure a.13 Absorption (blue) spectra and fit (red) of Er: YAG at 8K from 1525-1533nm…15

Table a.1 Lines believed to come from true ground state of Er^{3+} in YAG …….....16-18

Table a.2 Lines probably due to absorption from higher-lying states of $^4I_{15/2}$……18-20

7. Appendix

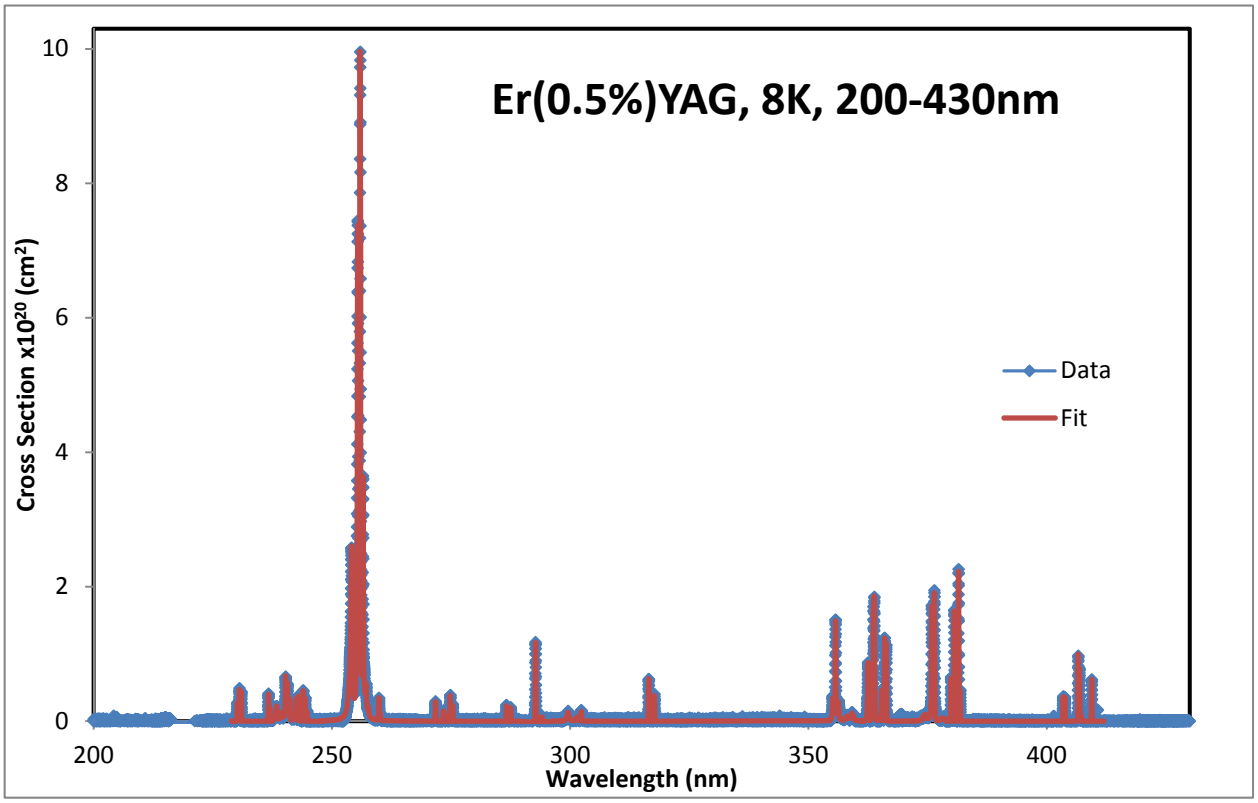

Figure a.1. Absorption (blue) spectra and fit (red) of Er: YAG sample at 8K from 200–430 nm.

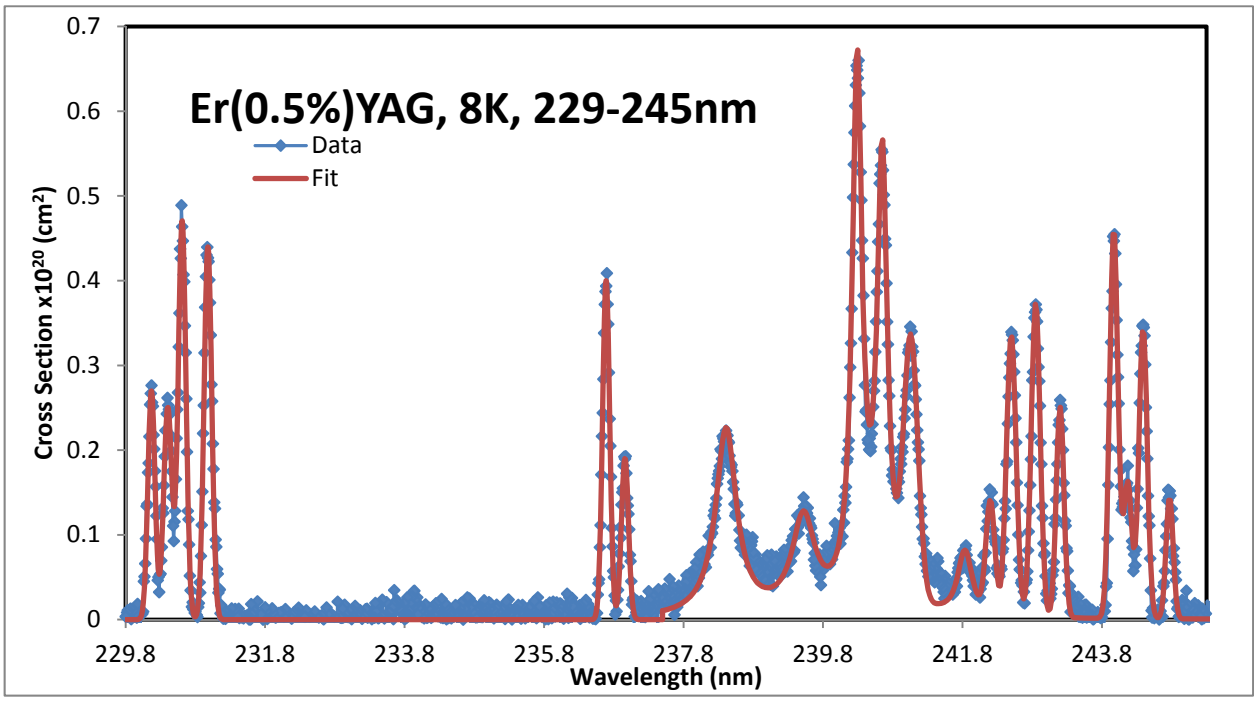

Figure a.2. Absorption (blue) spectra and fit (red) of Er: YAG sample at 8K from 229–245 nm.

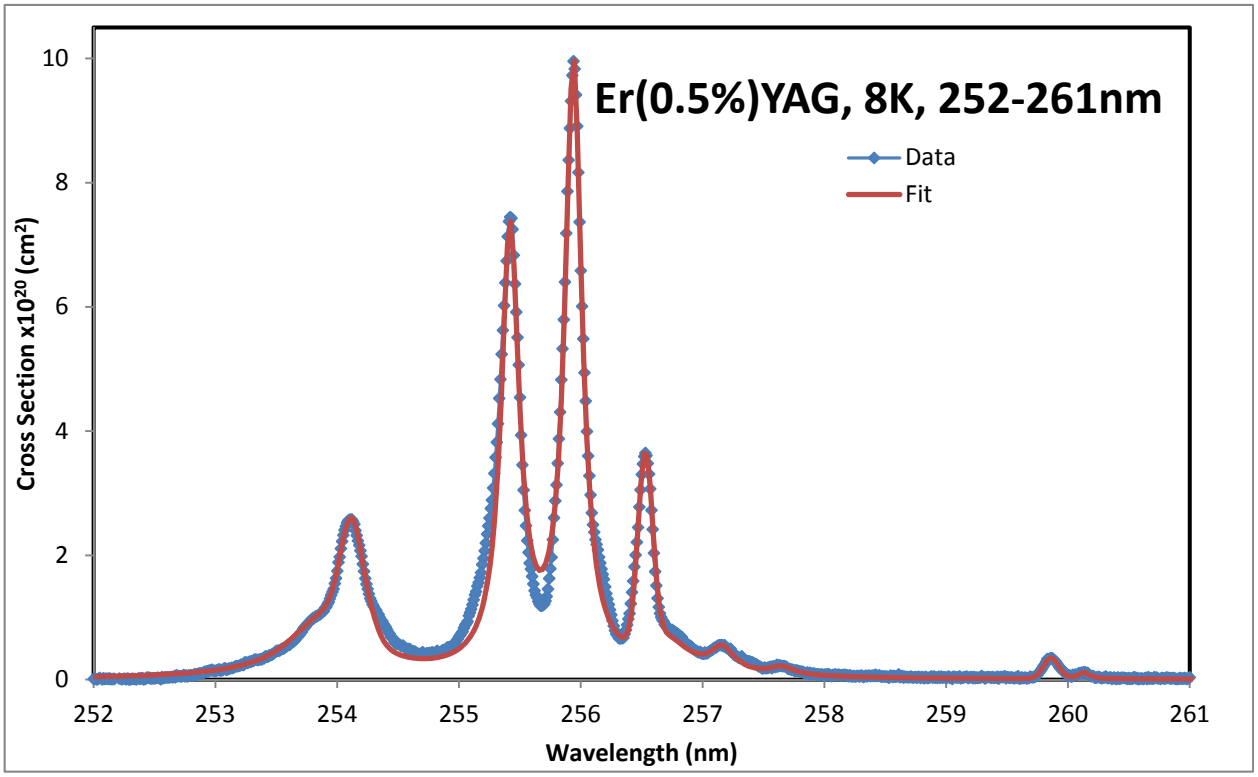

Figure a.3. Absorption (blue) spectra and fit (red) of Er: YAG sample at 8K from 252–261 nm.

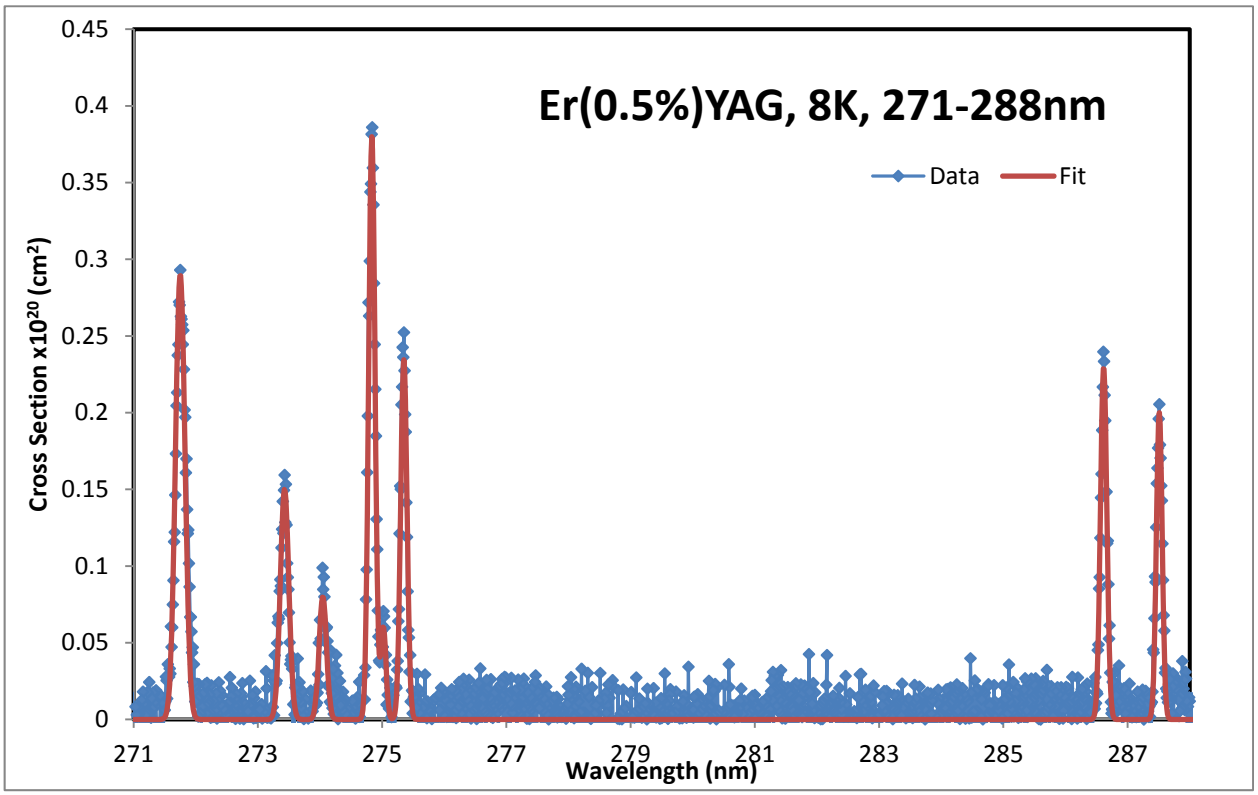

Figure a.4. Absorption (blue) spectra and fit (red) of Er: YAG sample at 8K from 271–288 nm.

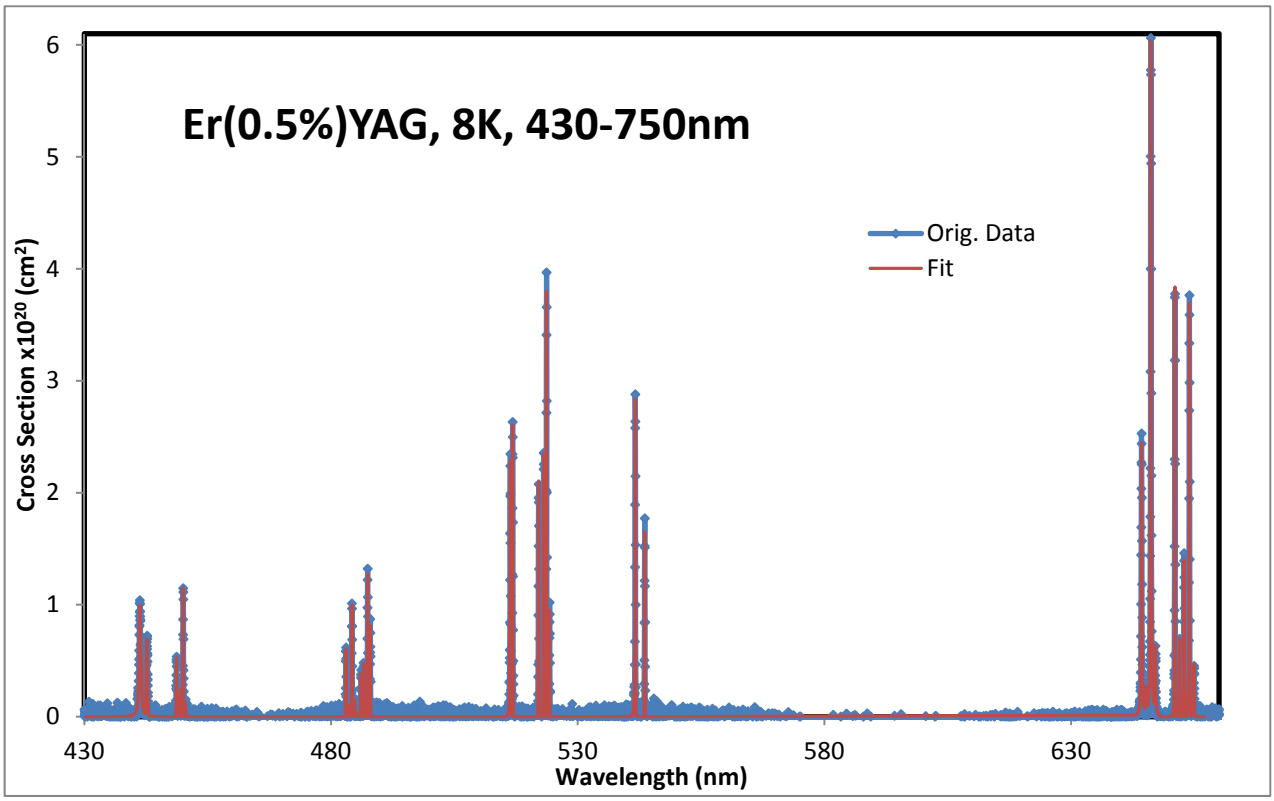

Figure a.5. Absorption (blue) spectra and fit (red) of Er: YAG sample at 8K from 430–750 nm.

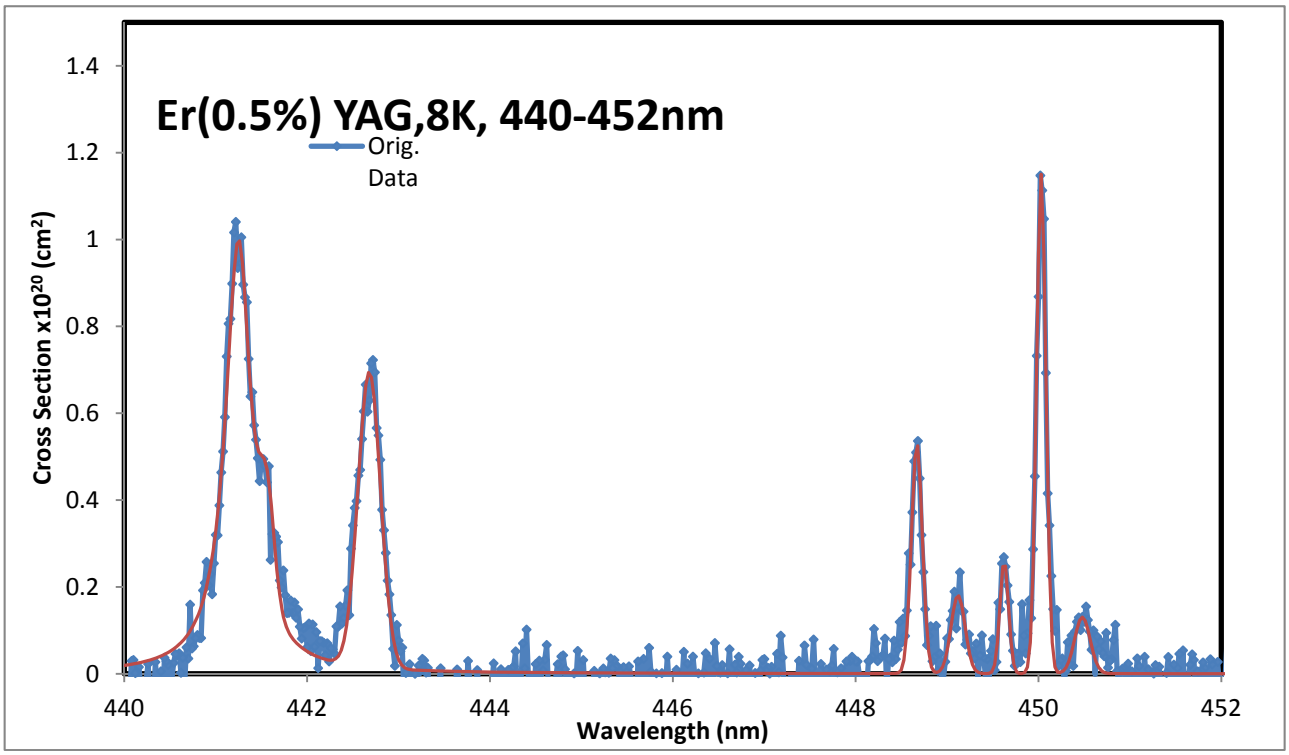

Figure a.6. Absorption (blue) spectra and fit (red) of Er: YAG sample at 8K from 440–452 nm.

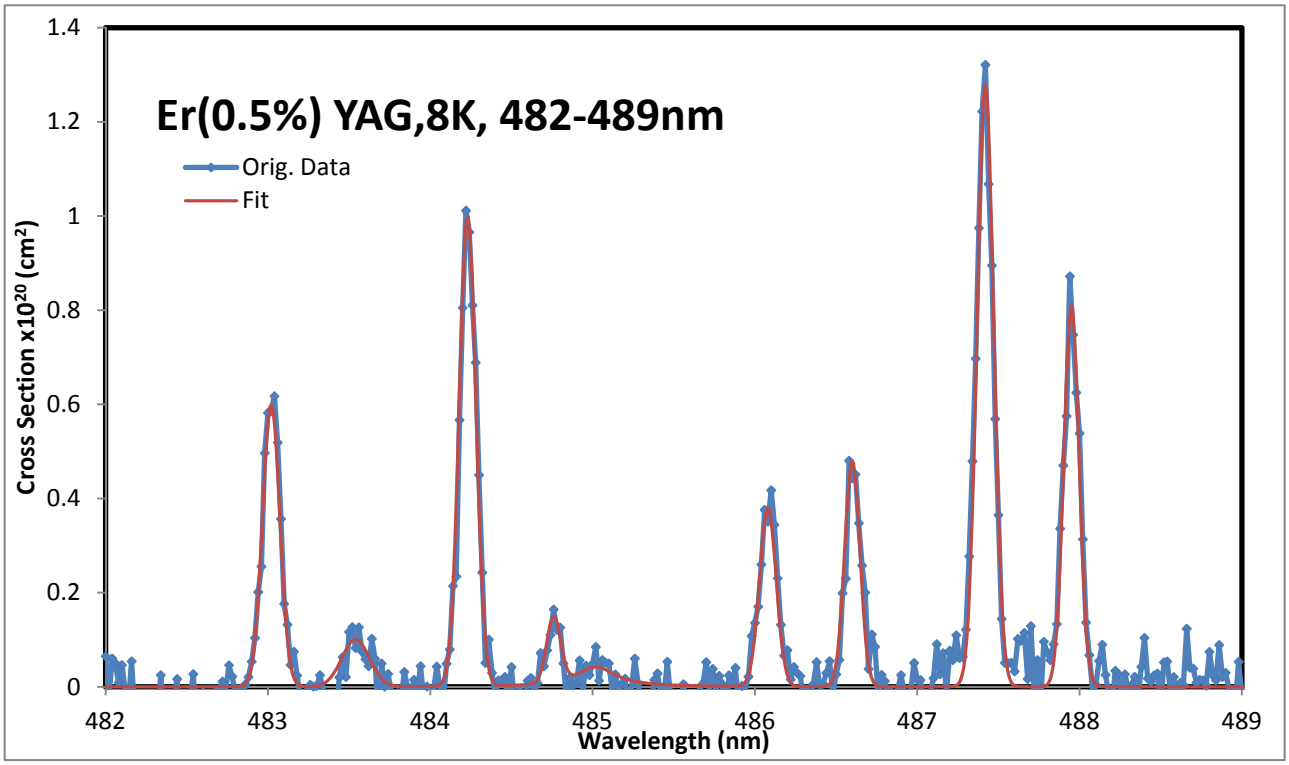

Figure a.7. Absorption (blue) spectra and fit (red) of Er: YAG sample at 8K from 482–489 nm.

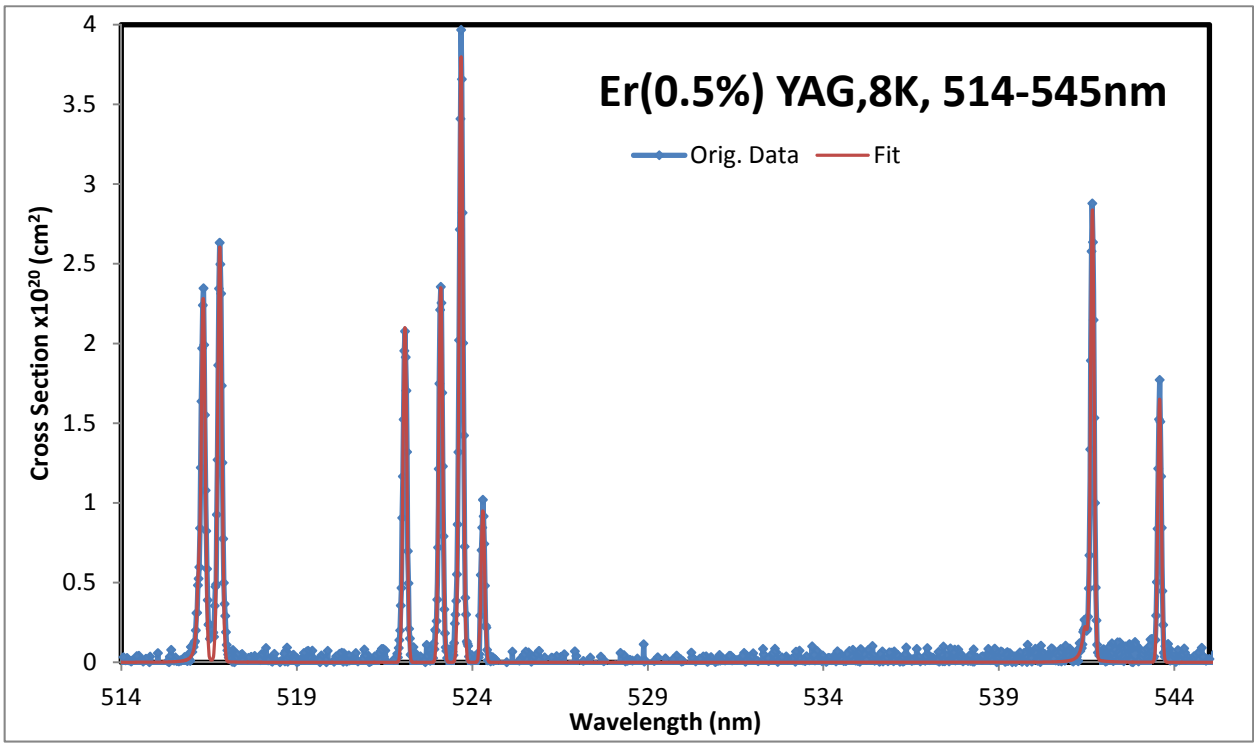

Figure a.8. Absorption (blue) spectra and fit (red) of Er: YAG sample at 8K from 514–545 nm.

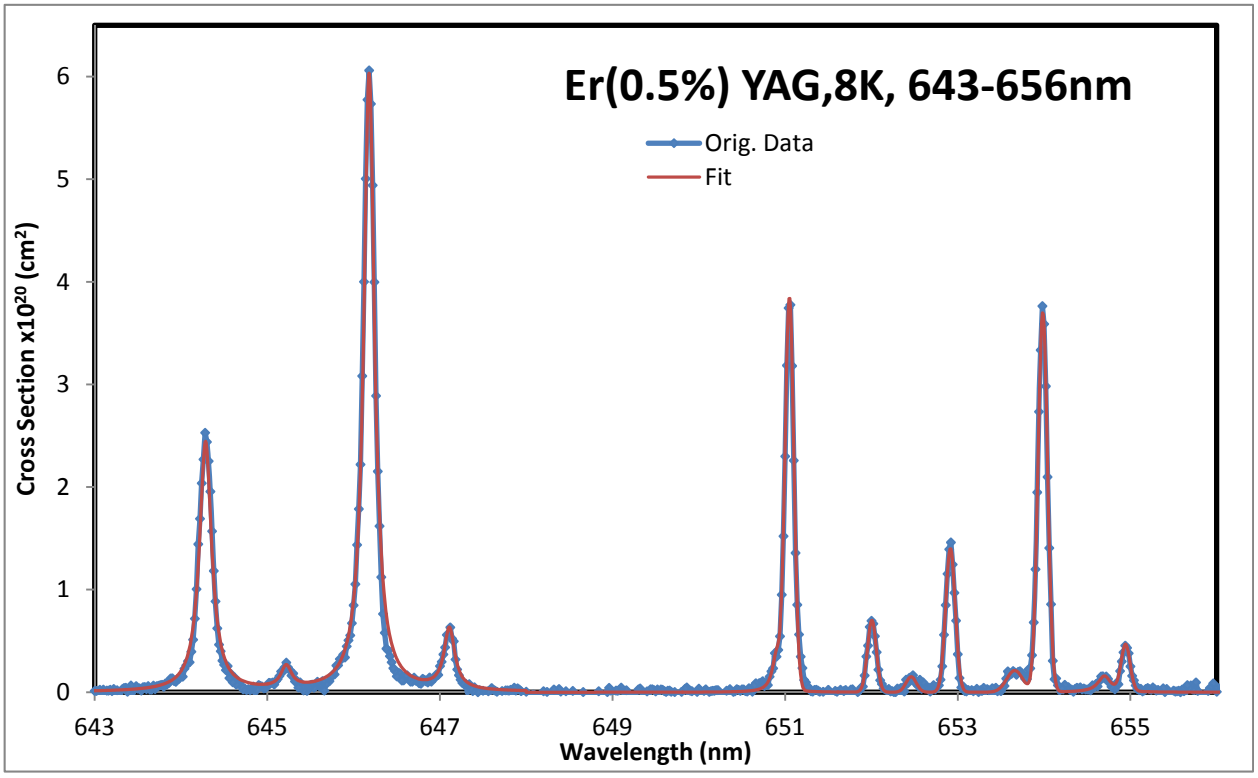

Figure a.9. Absorption (blue) spectra and fit (red) of Er: YAG sample at 8K from 643–656 nm.

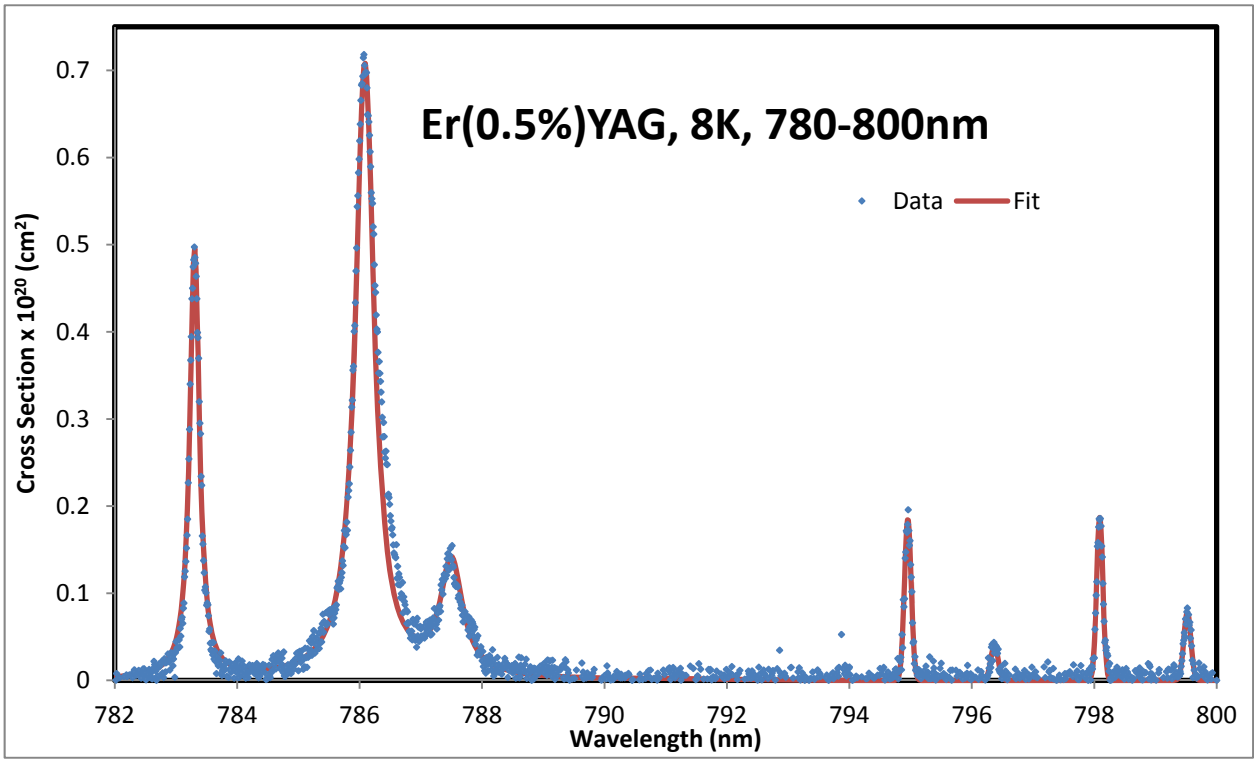

Figure a.10. Absorption (blue) spectra and fit (red) of Er: YAG sample at 8K from 780–800 nm.

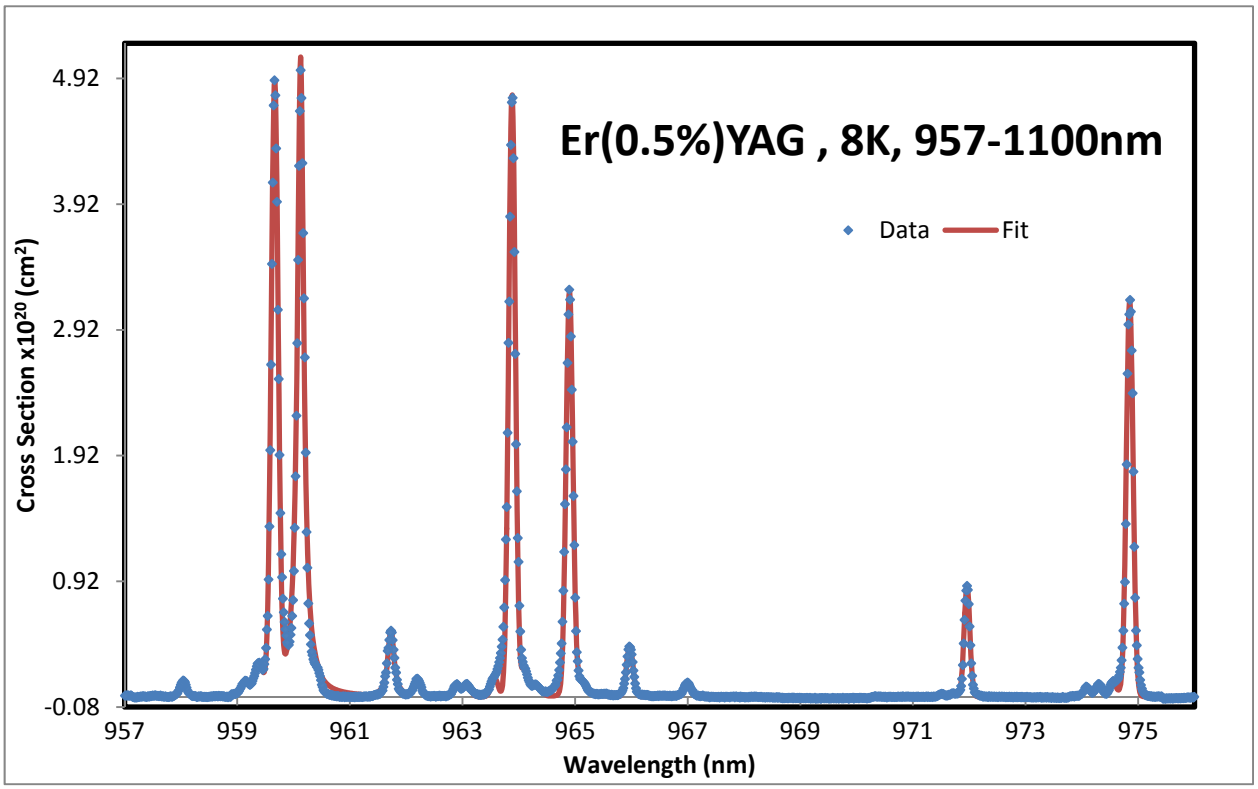

Figure a.11. Absorption (blue) spectra and fit (red) of Er: YAG sample at 8K from 957–1100 nm.

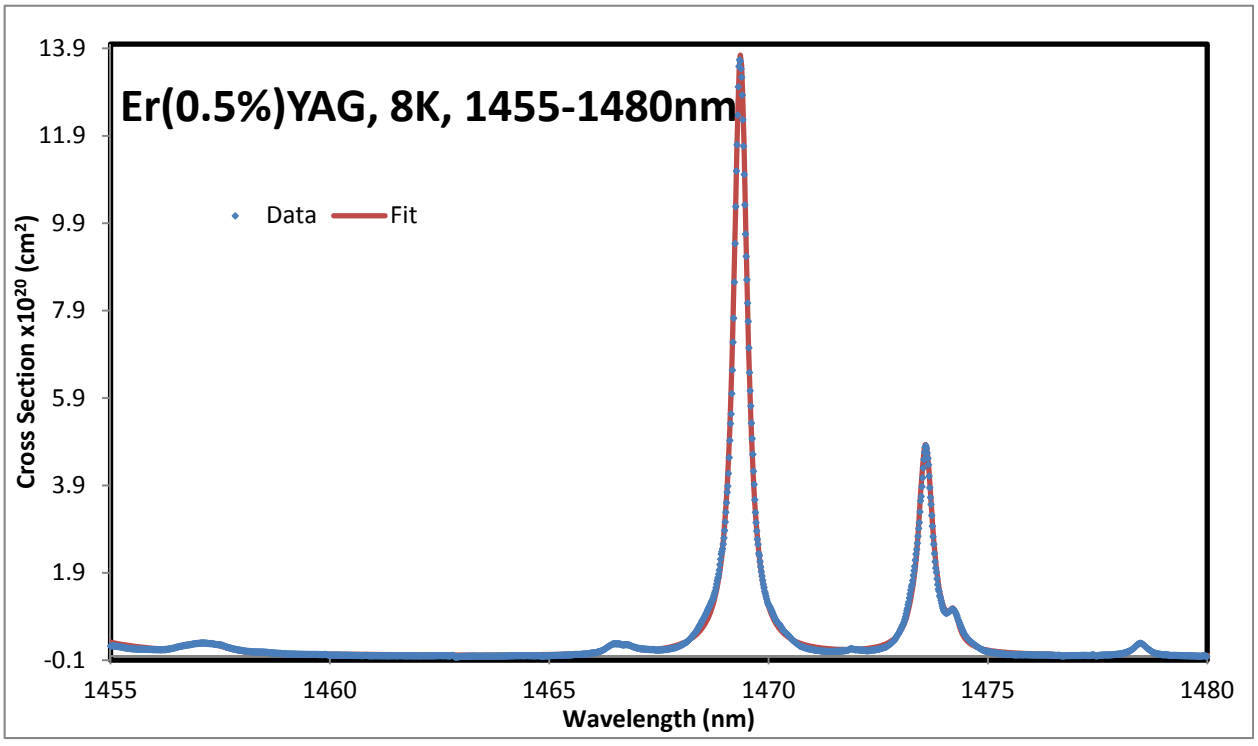

Figure a.12. Absorption (blue) spectra and fit (red) of Er: YAG sample at 8K from 1455–1480 nm.

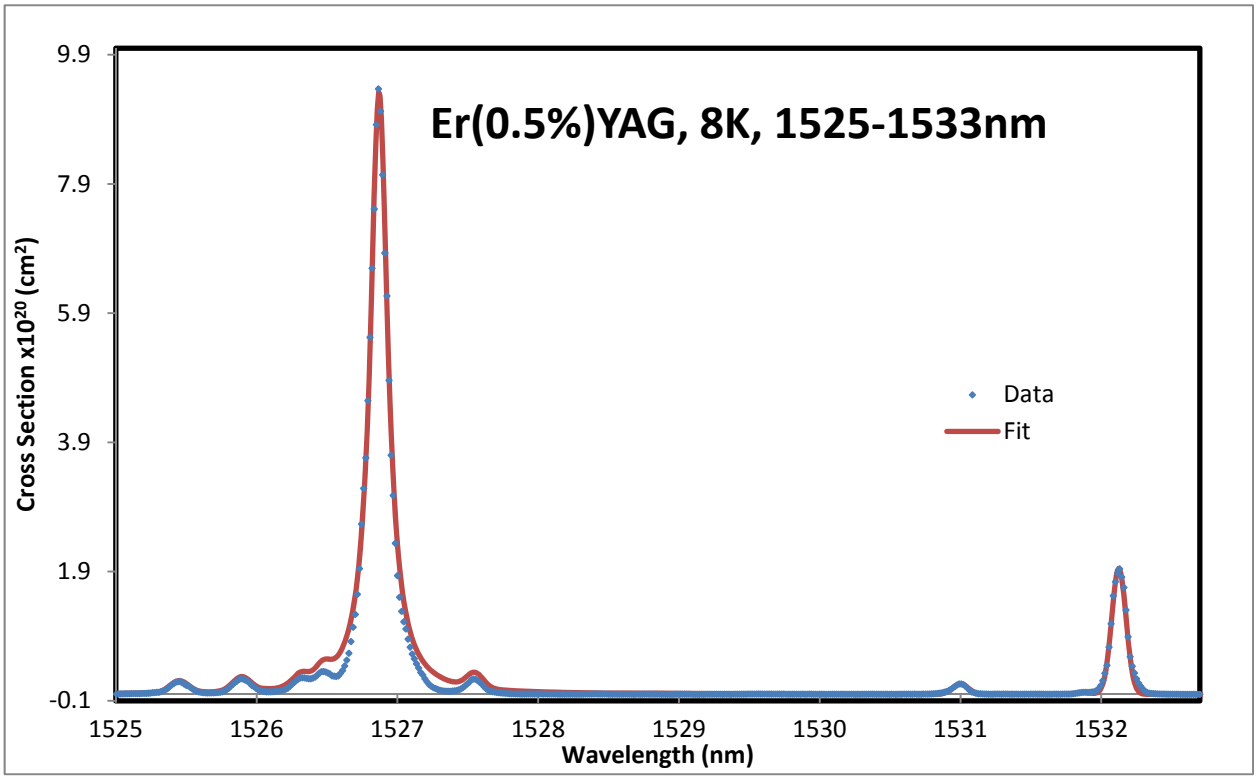

Figure a.13. Absorption (blue) spectra and fit (red) of Er: YAG sample at 8K from 1525–1533 nm.

Table a.1. Lines believed to come from true ground state of Er^{3+} in YAG.

	Absorption strengths and transition energies – 8K – Er:YAG							
Final manifold	No.	λ (nm)	σexpt (10^{-20} cm^2)	Line width (nm FWHM)	Area under peak expt (10^{-20})			
$^4I_{11/2}$		974.85	3.2	0.14	4.9			
		971.96	0.9	0.12	1.2			
		964.90	3.2	0.14	5.1			
		963.88	4.8	0.14	7.7			
		960.13	5.1	0.14	12			
		959.67	4.8	0.15	8.0			
$^4I_{9/2}$		812.68	0.96	0.12	1.9			
		798.09	0.19	0.12	0.38			

		794.96	0.18	0.13	0.40			
		786.09	0.70	0.37	6.6			
		783.31	0.49	0.19	2.4			
$^4F_{9/2}$		653.99	3.7	0.13	12			
		652.92	1.4	0.13	4.5			
		651.05	3.8	0.12	11			
		646.18	6.0	0.15	34			
		644.29	2.4	0.17	16			
4S3/2		543.58	1.6	0.12	7.1			
		541.67	2.8	0.12	12			
2H11/2		524.30	0.95	0.12	4.4			
		523.10	2.4	0.13	12			
		522.08	2.1	0.13	11			
		516.80	2.6	0.14	14			
		516.34	2.2	0.13	11			
		516.21	0.50	0.12	3.6			
4F7/2		487.42	1.3	0.12	6.9			
		486.08	0.38	0.12	2.0			
		484.23	1.0	0.12	5.4			
		483.02	0.60	0.13	3.4			
4F5/2		449.63	0.26	0.11	1.5 *			
		449.12	0.18	0.18	1.7			
		448.67	0.53	0.14	11			
4F3/2		442.68	0.68	0.29	11			
		441.25	1.0	0.35	28			
2G9/2		409.435	0.62	0.11	4.3 *			
		406.87	0.78	0.13	6.5			
		406.61	1.0	0.11	0.1 *			
		403.79	0.36	0.14	3.3			
		403.46	0.36	0.14	3.3			
4G11/2		381.5	2.2	0.12	20			
		380.59	1.6	0.11	13 *			
		379.93	0.64	0.12	5.7			
		376.42	1.9	0.18	25			
		376.2	shoulder	(not	resolved)			
		375.89	1.7	0.16	30			

2K15/2		366.32	1.2	0.13	12			
and		365.98	1.2	0.12	12			
4G9/2		365.39	0.45	0.14	7.5			
		363.81	1.9	0.12	26			
		363.65	1.5	0.11	13 *			
		363.21	0.4	0.11	3.3 *			
		362.51	0.8	0.12	7.7			
		362.39	0.3	0.16	5.9			
		not	found					
		359.15	0.11	0.58	7.8			
		358.08	0.06	0.73	5.5			
		not	found					
		not	found					
2G7/2		356.27	0.27	0.24	7.9			
		355.68	1.5	0.13	24			
		355.28	0.19	0.16	3.7			
		355.07	0.30	0.18	6.7			
2P3/2		317.69	0.38	0.11	4.4 *			
		316.48	0.63	0.14	9.4			
2K13/2 .		302.33	0.14	0.16	2.6			
2P1/2		301.53	0.07	0.40	4.5			
and								
4G5/2								
4G7/2		294.02	0.07	0.30	4.0			
		292.73	1.2	0.14	20			
2D(1)5/2		287.51	0.20	0.11	2.8 *			
		286.615	0.23	0.12	3.6			
2H(2)9/2		275.35	0.23	0.12	4.0			
		274.835	0.38	0.12	6.4			
		274.045	0.08	0.14	1.6			
		273.74	0.15	0.16	3.4			
		271.75	0.29	0.18	7.5			
4D5/2		260.13	0.10	0.11	2.7 *			
		259.86	0.33	0.14	7.5			
4D7/2		256.53	3.1	0.14	70			
		255.94	2.6	0.17	397			
		254.12	1.8	0.22	64			

2I11/2		244.77	0.14	0.12	3.0			
		244.39	0.34	0.14	8.5			
		244.17	0.16	0.14	4.0			
		243.97	0.46	0.14	12			
2L17/2 (?)		243.2	0.25	0.13	5.8			
		242.5	0.33	0.16	9.6			
2L17/2		242.2	0.13	0.15	3.5			
		241.06	0.30	0.24	13			
		240.65	0.53	0.18	26			
		240.29	0.64	0.17	29			
		239.52	0.11	0.40	12			
4D3/2		236.96	0.19	0.12	4.3			
		236.69	0.40	0.12	9.1			
2P3/2								
2I13/2		230.98	0.44	0.13	11			
		230.61	0.47	0.13	12			
		230.405	0.25	0.14	7.0			
		230.17	0.27	0.12	6.5			

* Area under peak may be in error by more than 10% due to finite resolution of instrument

** Area under peak may be in error by more than 30% due to finite resolution of instrument

Table a.2. Lines probably due to absorption from higher-lying states of $^4I_{15/2}$ (but may also include minority site peaks and/or vibronics).

	Absorption strengths and transition energies – 8K – Er:YAG							
Final manifold	No.	λ (nm)	σ_{expt} (10^{-20} cm^2)	Line width (nm FWHM)	Area under $peak_{expt}$ (10^{-20}			
$^4I_{11/2}$		974.56	0.13	0.14	0.28			
		974.30	0.09	0.13	0.13			
		974.08	0.08	0.13	0.17			
		966.99	0.12	0.14	0.19			
		965.97	0.40	0.14	0.62			
		965.10	0.13	0.24	0.54			
		964.30	0.10	0.20	0.23			
		964.10	0.23	0.13	0.34			

		963.57	0.15	0.14	0.24			
		963.08	0.10	0.16	0.18			
		962.89	0.10	0.14	0.15			
		962.20	0.13	0.14	0.20			
		961.73	0.54	0.13	1.2			
		955.68	0.16	0.78	2.2			
		959.38	0.24	0.17	0.46			
		959.14	0.10	0.17	0.20			
		958.04	0.13	0.13	0.19			
$^4I_{9/2}$		814.16	0.11	0.12	0.21			
		812.45	0.03	0.16	0.11			
		799.52	0.08	0.14	0.18			
		787.50	0.13	0.44	1.45			
$^4F_{9/2}$		654.95	0.45	0.12	1.3			
		654.70	0.16	0.18	1.0			
		653.66	3.7	0.13	1.2			
		652.46	0.15	0.14	0.52			
		652.00	0.70	0.12	2.1			
		650.90	0.37	0.12	1.7			
		647.11	0.64	0.14	3.3			
		645.22	0.21	0.15	1.2			
$^4S_{3/2}$		541.46	0.22	0.20	2.4			
$^2H_{11/2}$		523.68	3.8	0.13	19			
$^4F_{7/2}$		487.94	0.81	0.11	4.0 *			
		486.60	0.48	0.11	2.4 *			
		485.02	0.04	0.30	0.85			

* Area under peak may be in error by more than 10% due to finite resolution of instrument

** Area under peak may be in error by more than 30% due to finite resolution of instrument

Appendix E. Coherent Combination of Fiber MOPAs Seeded by a Chirped Laser

This appendix is presented in its original form without editorial change.

U.S. Army Research Laboratory

SUMMER RESEARCH TECHNICAL REPORT

Coherent Combination of Fiber MOPAs Seeded by a Chirped Laser

Zhi Yi Yang

Mentor: Jeffrey O. White

Microphotonics Branch

Electro-optics and Photonics Division

Sensors and Electron Devices Directorate

Abstract

In order to aid in the development of high-power, weapons-grade lasers, we investigated coherent beam combining and suppression of stimulated Brillouin scattering. Scaling a single laser to higher powers is becoming increasingly more complex and expensive, but by coherently combining ten 10-kW lasers, or twenty 5-kW lasers, one can create an equivalent 100kW laser at lower cost and complexity. By chirping the frequency of the laser in a highly linear fashion, stimulated Brillouin scattering is suppressed while still allowing efficient phase locking. In this experiment, a chirped diode laser seeds two 10W Er fiber amplifiers which are coherently combined by an opto-electronic phase-locked loop. We are able to show beam combining with path length differences up to 30cm while maintaining at least 90% efficiency.

1. Introduction/Background

High energy lasers in the range of 100kW or higher are desirable, but due to the complexity, size, and cost, have not gone beyond the prototype stage. Most complexities are due to thermal management and compensating for thermal effects, especially in bulk lasers. Scaling lasers is not always simply a matter of increasing the pump power as that will eventually sacrifice other aspects of the laser performance like beam quality or will exacerbate thermal effects, therefore beam combining is becoming an attractive alternative (*1*). Beam combining scales power by combining a number of laser modules to produce a single output beam. This method has the advantage of keeping the high beam quality associated with lower power lasers while obtaining a high power beam.

Fiber lasers are an appealing laser system due to their ease in thermal management and relatively high electrical to optical efficiency. Their compactness also means smaller overall final packages can be made. At the same time because of its small core size and long lengths, nonlinear effects occur more readily. A well known nonlinear effect that limits the power in fibers is stimulated Brillouin scattering (SBS). Methods used to suppress SBS often involve broadening the linewidth which unfortunately makes beam combining difficult due to shortening the coherence length. Recent developments in beam combining at Northrop Grumman show that a kilowatt range fiber amplifier can be coherently combined (*2*). One of the major limiting factors for practical beam combining is the path length of the fibers must be matched well to within the coherence length. For a laser that has a linewidth of 10 MHz, the coherence length in fiber is approximately 20 meters. Northrop Grumman broadened their laser linewidth to 25GHz in order to suppress the SBS at that power level. This has required them to path length match their fibers to well below the coherence length of 8 mm in order to achieve a 90% beam combining efficiency. By frequency chirping our laser, suppression of SBS (*3*) can be achieved while still being able to coherently combine (*4*). This method of SBS suppression allows us to maintain at least 90% combining efficiency with a path length difference two orders of magnitude longer than previously achieved. Instead of requiring every amplifier to be path length matched to within a few millimeters, this method will tolerate mismatches in the range of tens of centimeters. This makes fabrication of such systems and replacement of individual elements in the field easier. These factors make coherent beam combining practical.

Beam combining can be done spectrally or coherently. Spectral combining involves beams of different wavelengths overlapping without any phase control. Coherent beam combining (CBC) uses beams at the same wavelength, and with phase control, have the beams interfere constructively. Although CBC is more difficult to implement, the brightness of the combined beams scales as N^2 rather than N, where N is the number of beams combined (*5*). The N^2 scaling makes CBC attractive, because in military applications, the effective range is related to the

brightness (*6*). CBC is implemented through the use of a phase controller and feedback loop. In our experiment, the phase-locked loop (PLL) technique is used as the feedback loop along with an acousto-optic frequency shifter (AOFS) as the phase/frequency controller.

A PLL is a negative feedback circuit which adjusts the output signal to match the phase of a reference signal. A typical PLL consists of a phase detector, filter and a voltage controlled oscillator (VCO [*7*]). The phase detector compares the reference with the output and generates an error signal whenever the two do not coincide. The error signal adjusts the VCO so that when in lock, the frequency difference is zero. The filters help determine the characteristics of the PLL such as loop bandwidth, and hold-in range (*8*).

Narrow linewidth, single mode lasers are used for CBC due to their long coherence length. This eases the requirement for high beam combining efficiency but suffers from SBS. Confinement of the light inside a fiber core leads to high intensity, this, in combination with a long path length provides ideal conditions for SBS. By broadening the linewidth (much greater than the Brillouin linewidth) this can be avoided, but would limit the possible path length difference between each channel that was afforded by the original narrow linewidth laser.

SBS builds from spontaneous Brillouin scattering of a laser photon from a thermally generated acoustic phonon in the fiber. This is an inelastic collision, meaning there is an energy transfer that shifts the scattered photon up or down in frequency by the acoustic frequency. Because single mode fibers are a waveguide, the scattered photon will be guided either forward or backwards only. At high enough forward laser power this spontaneous process builds up to become stimulated. As the scattered photon propagates backward it interacts with the forward propagating beam, creating a traveling wave. Through the phenomenon of electrostriction (*9*), this interaction between the forward and backward propagating beams can alter the density of the fiber. This induces a periodic modulation of the refractive index that can scatter more of the forward propagating beam. As this process propagates down the fiber it will build up the intensity of the backwards beam which will limit the forward laser intensity, and can become intense enough to damage the laser. The forward propagating scattered photons do not see this amplification due to a lack of phase matching between the acoustic, laser, and stokes waves. Our laser suppresses SBS by sweeping the laser frequency; shifting the Brillouin frequency of the backward propagating beam off resonance, preventing it from efficiently generating acoustic waves that can scatter more light. This is similar to having a broad linewidth laser that decreases the strength of the phase matching process thereby increasing the threshold for SBS. Our process is more effective than this random broadening of the laser linewidth because the resonance frequency is shifting away from the Stokes frequency in a well defined manner (*10*).

For coherent combining, the linearity of the chirp is important. The chirped diode laser sweeps the frequency linearly, so as to minimize the bandwidth required of the PLL. When the laser is split into two paths with a given path length difference they have a constant frequency offset when linearly chirped. The PLL would only need a single frequency correction for this situation.

For nonlinear chirps, the offset is continuously shifting, requiring multiple correction from the PLL. Therefore the more nonlinear the chirp is, the more bandwidth the PLL will require. A Mach-Zehnder interferometer is used to measure the linearity of the chirp. The chirp signal is split into two paths where one path has a delay. The signals from the two paths will then recombine on a photodiode. The closer the chirp is to being linear, the closer the signal the photodiode generates is a pure sinusoid.

2. Experiment/Calculations

Our chirped diode laser (Caltech, Telaris) has a nominal wavelength of 1.5 μm and is split into three channels (figure 1). The first is used as a reference while the other two channels have acoustic-optic frequency shifters (AOFS) that control the frequency of the beams, and thus their phase. Our AOFSs shift the channels by a nominal 100 MHz to serve as a heterodyne signal, allowing for it to be easily separated from low frequency noises. Each of the two channels is then amplified by a polarization maintaining (PM) erbium-doped fiber amplifier (EDFA) (Nufern) which has a 16 m delivery fiber. The amplifiers have a polarization extinction ratio of 10 dB. After the two beams are collimated they are reflected by an anti-reflection coated wedge where they each mix with the reference beam on a separate photodetector. The photodetector sees a beat frequency of 100 MHz from the AOFS. The PLL compares the beat signal to an onboard 100 MHz oscillator. Any path length difference between a channel and the reference will create a frequency offset from this beat signal. This causes the PLL to generate error signals that drive the AOFS to correct the discrepancy. This setup locks each beam independently to the same reference beam rather than directly to each other.

The signal from the photodetector is also captured by an oscilloscope, and later demodulated in order to quantify the residual phase error. The transmitted beams from the wedge are combined by having the two beams at a slight angle to one another so that they will overlap in the far field, forming a fringe pattern. The number of fringes is dictated by the angle between the beams, where the larger the angle the more fringes appear. The beam profile is then captured by an IR camera. Using the images captured by the camera, the visibility is calculated. The visibility is another method to quantify the combining efficiency.

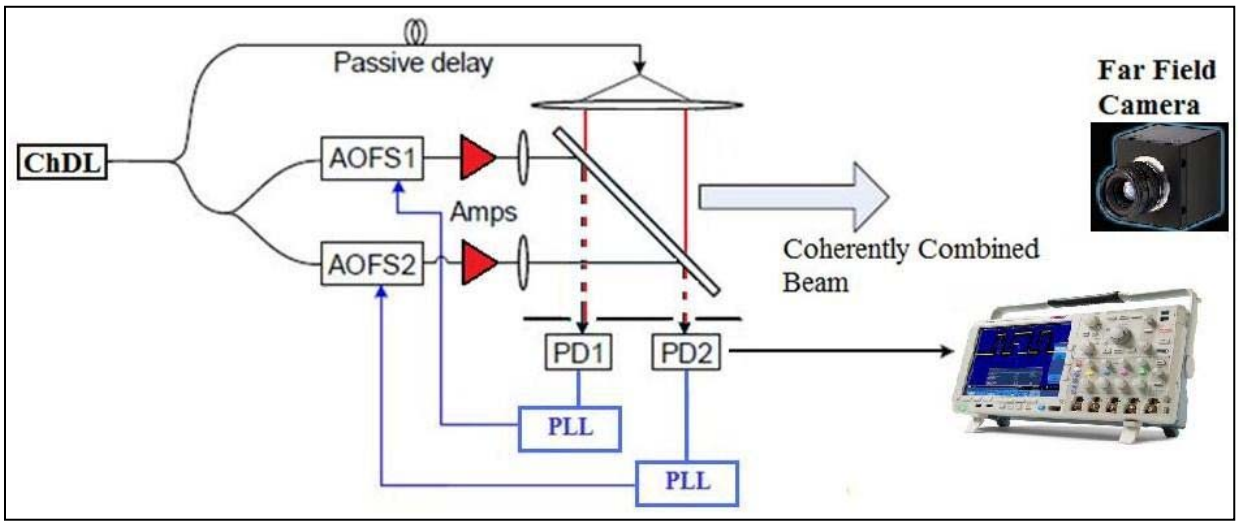

Figure 6. Schematic of coherent beam combining experiment. Chirp diode laser(ChDL), Acoustic-optic frequency shifter (AOFS), Photodetector(PD), Phase Lock-loop(PLL).

3. Results and Discussion

The efficiency of beam combining is partly determined by how much residual phase error there is between the channels. Therefore, the more residual phase error there is the lower the combining efficiency. Other sources from the setup that affect the combining efficiency are the degree of overlap of the reference and the channel beam on the photodetector, the overlap between the channels in the far field, how well the polarizations are aligned, intensity matching between the channels, any wavefront distortion, and the amount of gain on the PLL. Random noise sources (*11*) cause small path length differences between the channels that need to be corrected by the PLL. These sources are from thermal fluctuations in the fiber and vibrations (acoustic/mechanical) from the environment.

A measurement of residual phase error was done with the time traces of the beat frequency that were captured by the oscilloscope. The time trace of a chirp is demodulated using I/Q demodulation in postprocessing. The phase at the photodetector is then calculated by taking the tangent of the ratio of the I and Q demodulation. The phase difference between the channels is calculated and the standard deviation is used to calculate the combining efficiency. The combining efficiency can be calculated by[5]:

$$\eta_c = 1 - \frac{N-1}{N}\sigma^2 ,$$

assuming phase fluctuations are the only error source, where N is the number of beams and σ is the standard deviation of the residual phase error. The following phase error measurement was

done without the EDFA. The figure below shows the error is proportional to the path length difference between the reference and each channel. As stated before we are interested in the error between the two channels. Although the figure shows the phase error between the reference and the channels, one of the channels (blue) is path length matched to the reference and not varied. The phase error by OPLL1 (red) is the dominate error and can be taken as the total phase error between the two channels.

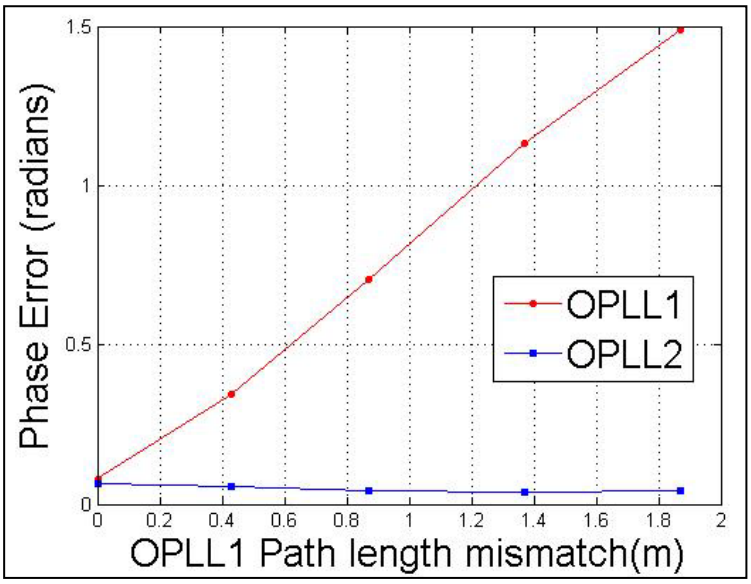

Figure 7. Residual phase error relative to the reference, as a function of OPLL1 path length mismatch, OPLL2 and the reference are path length matched.

The next measurement is done with the EDFA while maintaining the same path length difference and increasing the pump power. The following graph shows that the EDFA does not contribute much to the phase error. This shows that random intensity noise, amplified spontaneous emission, and self-phase modulation are not a problem at these power levels in these amplifiers. This is true up to when SBS occurs, at which point the intensity noise increases, causing momentary phase slips. These slips occur because the loop gain is proportional to the intensity on the photodiodes. SBS can cause phase noise to increase because it takes power away from the forward beam in an unstable manner, causing the intensity to fluctuate.

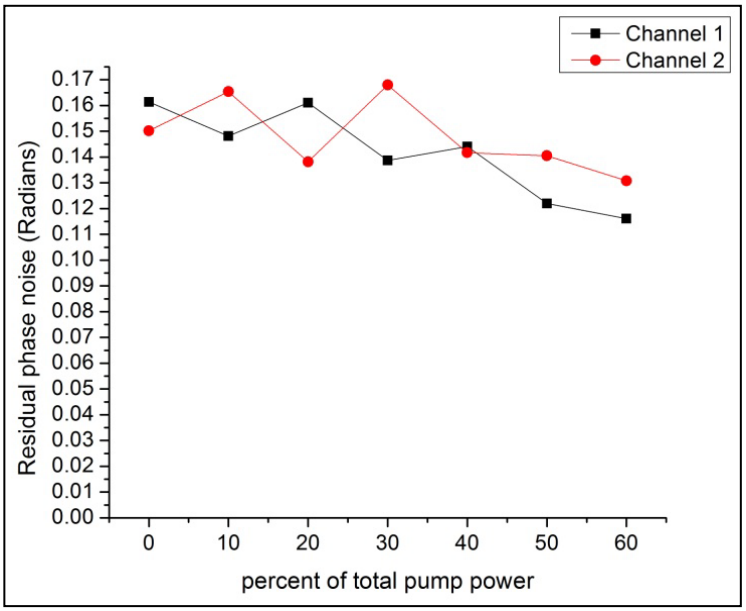

Figure 8. Residual phase error vs the percent of total pump power. The chirp rate is $2x10^{14}$ Hz/s. Higher pumping results in SBS which increases the phase noise.

Another method to measure the combining efficiency would be to measure the visibility. Unlike the oscilloscope method this measures the combining efficiency over several chirp periods including the transient parts where the PLL loses lock. As noted before, the chirped diode laser chirps the frequency in a triangular waveform. Whenever a turnaround point occurs, a sudden change in the beat frequency will occur causing the PLL to lose lock momentarily. Although the beams combine incoherently when the PLL loses lock, the unlocked time is short compared to the times the PLL is locked.

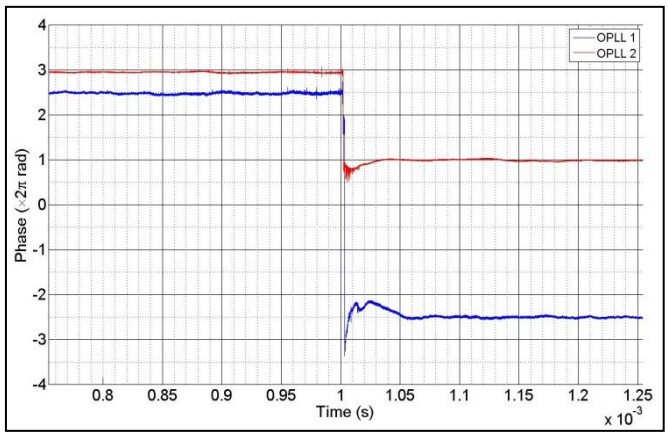

Figure 9. Transient crossover time trace for chirp rate $5x10^{14}$ Hz/s.

The time traces above include the transients where the PLL looses lock. During these transients, there can be a large arbitrary jump in phase that is a multiple of 2π. Since our oscilloscope

method uses the standard deviation of the time traces to calculate the residual phase error, we should avoid these sections of time. The length of time to relock varies from 30-100 μs depending on the gain of the PLL. This accounts for no more than 10% of the 1 ms chirp period for the chirp of $5x10^{14}$ Hz/s. The visibility is defined by[1]:

$$V = \frac{I_{max} - I_{min}}{I_{max} + I_{min}}$$

The I_{max} corresponds to the peak intensity captured by the camera. The I_{min} is the null intensity which can be obtained at the same spot of the peak intensity by π-shifting the phase of one channel.

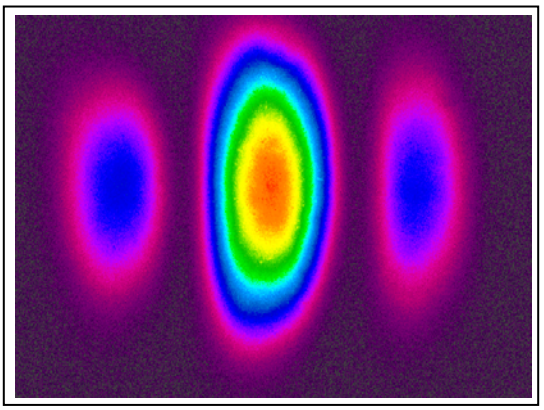

Figure 10. Coherent combining with 0 degree offset.

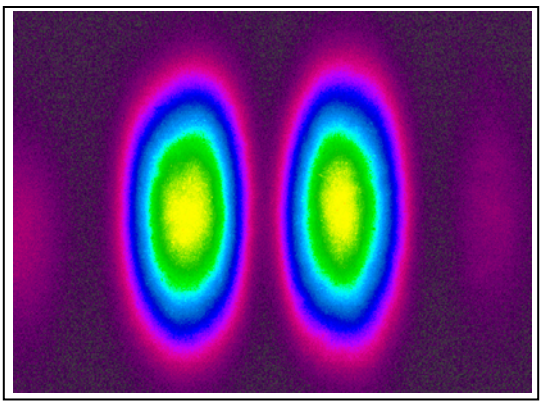

Figure 11. Coherent combining with 180 degree offset.

At a chirp of $5x10^{14}$ Hz/s, and 3W beams, data was taken for a path length difference of 34 cm between the two channels. The residual phase error measured using the time trace was 0.135 rad. Using the combining efficiency equation a 99% efficiency was achieved while having two orders of magnitude longer in path length difference than previous attempts[1]. Using the visibility equation the combining efficiency is approximately 90%. This difference is mostly due to the transient time when the beams are combining incoherently. Other contributing factors to the

decoherence are the beam overlap, intensity matching, and any wavefront distortion from imperfect optics. Using the time traces to quantify the combining efficiency gives a narrow view of the performance of mainly the chirp diode laser, amplifiers, and PLL. Whereas using the visibility gives an overall performance level.

Lastly, the highest power beam combining was done at 7W while the laser was chirping at $5x10^{14}$Hz/s. The path length mismatch was ~30 cm with a combining efficiency of 93% using the time traces, rather than 99% obtained at 3 W. The decrease in combining efficiency is due to SBS, which could be suppressed a higher chirp. There is unfortunately not enough bandwidth for this PLL to work effectively at higher chirps. As the chirp increases, the times the beams combine incoherently becomes more significant.

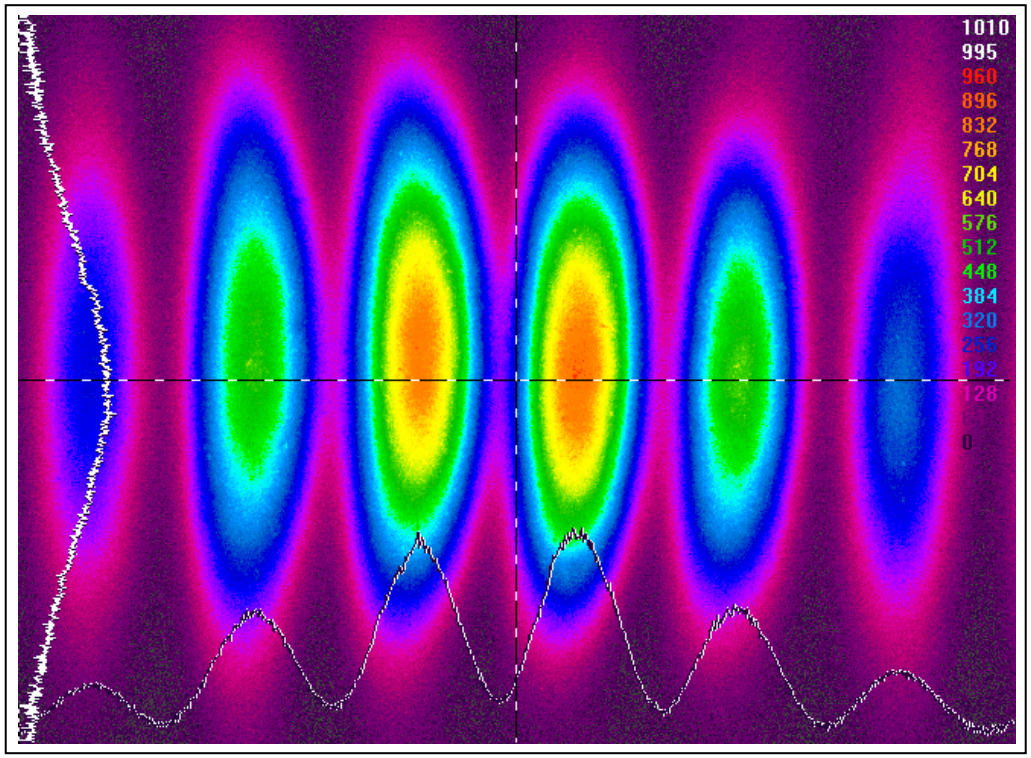

Figure 12. Fringe pattern from coherent beam combining captured on camera. Each beam is 7 W and chirping at $5x10^{14}$ Hz/s. The path difference between channel 1 and 2 is approximately 30 cm.

4. Summary and Conclusions

We were able to show that CBC is possible even when the two interfering beams are changing frequency at 5×10^{14} Hz/s. This technique has relaxed the requirement of having the channels closely path length matched. We were able to maintain combining efficiency above 90% at path length differences of 30 cm between channels. In the experiment that combined 7 W beams, the chirp of $5x10^{14}$ Hz/s was not enough to suppress SBS entirely and thereby reduced the combining efficiency. This shows that the limiting factors in the system are the chirp rate and the bandwidth of the PLL.

We would need higher chirp rates when working in the kilowatt range and a larger bandwidth in order to reduce the locking time. We are continuing this work by moving to Ytterbium fiber amplifiers at the kilowatt level. For this, we are developing a 1.06 μm laser that can chirp at higher rates ($>10^{15}$ Hz/s) that will be able to suppress SBS for much higher power. At this power level we will also investigate other nonlinear effects such as self-phase modulation.

5. References

1. Augst, Steven J.; Fan, T. Y.; Sanchez, Antonio. Coherent Beam Combining and Phase Noise Measurements of Ytterbium Fiber Amplifiers. *Opt. Lett.* **2004**, *29*, 474–476.

2. Goodno, Gregory D.; McNaught, Stuart J.; Rothenberg, Joshua E.; McComb, Timothy S.; Thielen, Peter A.; Wickham, Michael G.; Weber, Mark E. Active Phase and Polarization Locking of a 1.4 kW Fiber Amplifier. *Opt. Lett.* **2010**, *35*, 1542–1544.

3. White, J. O.; Vasilyev, A.; Cahill, J. P.; Rakuljic, G.; Satyan, N.; Mungen, C. E.; Yariv, A. Suppression of Stimulated Brillouin Scattering in Optical Fibers Using a Linearly-Chirped Diode Laser. *Optics Express* **2012**, *20*, 15881.

4. Satyan, N.; Vasilyev, A.; Rakuljic, G.; White, J. O.; Yariv, A. Phase-locking and Coherent Power Combining of Broadband Linearly Chirped Optical Waves. *Optics Express* **2012**, *20*, 25213.

5. Fan, T. Y. Laser Beam Combining for High-power, High-radiance Sources. *Selected Topics in Quantum Electronics IEEE Journal of* **May–June 2005**, *11* (3), 567–577.

6. Goodno, G. D.; Asman, C. P.; Anderegg, J.; Brosnan, S.; Cheung, E. C.; Hammons, D.; Injeyan, H.; Komine, H.; Long, W. H.; McClellan, M.; McNaught, S. J.; Redmond, S.; Simpson, R.; Sollee, J.; Weber, M.; Weiss, S. B.; Wickham, M. Brightness-Scaling Potential of Actively Phase-Locked Solid-State Laser Arrays. *Selected Topics in Quantum Electronics. IEEE Journal of* **May–June 2007**, *13* (3), 460–472.

7. Horowitz, Paul; Hill, Winfield. *The Art of Electronics*. Cambridge University Press, 1989.

8. Satyan, Naresh. *Optoelectronic Control of the Phase and Frequency of Semiconductor Lasers*. PhD dissertation, California Institute of Technology, Pasadena, CA, 2011.

9. Kobyakov, Andrey; Sauer, Michael; Chowdhury, Dipak. Stimulated Brillouin Scattering in Optical Fibers. *Advances in Optics and Photonics* **2010**, *2*, Issue 1, 1–59.

10. Mungan, C. E.; Rogers, S. D.; Satyan, N.; White, J. O. Time-dependent Modeling of Brillouin Scattering in Optical Fibers Excited by a Chirped Diode Laser. to be published in IEEE Journal of Quantum Electronics.

11. Augst, Steven J.; Fan, T. Y.; Sanchez, Antonio. Coherent Beam Combining and Phase Noise Measurements of Ytterbium Fber Amplifiers. *Opt. Lett.* **2004**, *29*, 474–476.

INTENTIONALLY LEFT BLANK.

List of Symbols, Abbreviations, and Acronyms

ARL	U.S. Army Research Laboratory
DEPS	Directed Energy Professional Society
ECE	Electrical and Computer Engineering
EE	electronic engineering
HEL	High Energy Laser
JTO	Joint Technology Office
LMA	large mode area

NO. OF COPIES	ORGANIZATION
1 (PDF)	DEFENSE TECHNICAL INFORMATION CTR DTIC OCA 8725 JOHN J KINGMAN RD STE 0944 FORT BELVOIR VA 22060-6218
1 (HC)	DIRECTOR US ARMY RESEARCH LAB IMAL HRA 2800 POWDER MILL RD ADELPHI MD 20783-1197
1 (PDF)	DIRECTOR US ARMY RESEARCH LAB RDRL CIO LL 2800 POWDER MILL RD ADELPHI MD 20783-1197
1 (PDF)	GOVT PRINTG OFC A MALHOTRA 732 N CAPITOL ST NW WASHINGTON DC 20401

ADELPHI LABORATORY CENTER

1 (PDF)	DIR USARL RDRL SEE M J WHITE